

AD-A181 824

PRODUCT-STATE-RESOLVED KINETIC STUDY OF THE  $H(+)$  +  $F(-)$

1/1

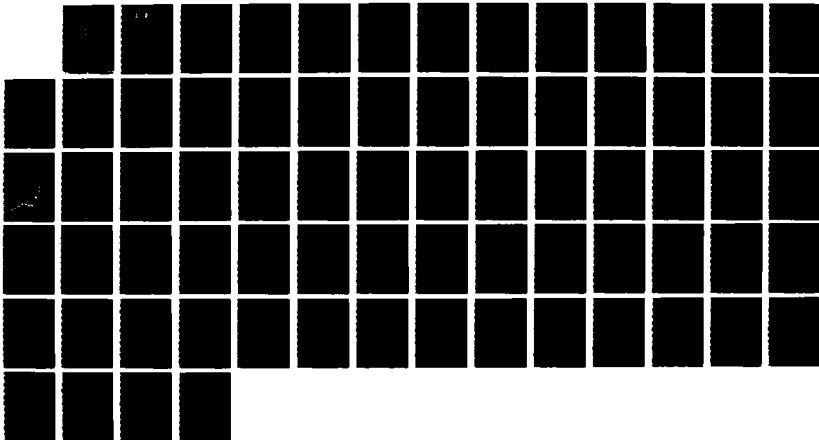
ION-ION REACTION(U) NAVAL RESEARCH LAB WASHINGTON DC

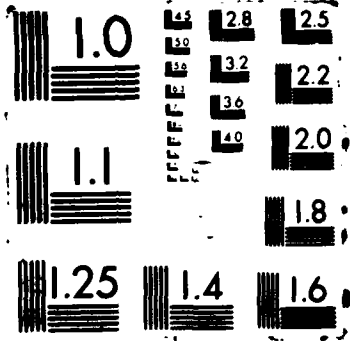
H WANG 18 DEC 86 AFOSR-TR-87-0663 AFOSR-MIPR-86-00007

F/G 7/2

NL

UNCLASSIFIED





unclas  
SECURITY CL

DOCUMENTATION PAGE

AD-A181 824

1a. REPORT  
unclas

1b. RESTRICTIVE MARKINGS

2a. SECURITY CLASSIFICATION AUTHORITY

3. DISTRIBUTION / AVAILABILITY OF REPORT

2b. DECLASSIFICATION / DOWNGRADING SCHEDULE

Approved for public release;  
Distribution unlimited

JUN 24 1987  
D

4. PERFORMING ORGANIZATION REPORT NUMBER(S)

5. MONITORING ORGANIZATION REPORT NUMBER(S)

AFOSR-TM- 87-0668

6a. NAME OF PERFORMING ORGANIZATION

6b. OFFICE SYMBOL  
(if applicable)

7a. NAME OF MONITORING ORGANIZATION

Naval Research Laboratory

Code 6180

AFOSR/NC

6c. ADDRESS (City, State, and ZIP Code)

7b. ADDRESS (City, State, and ZIP Code)

Washington, D. C. 20375-5000

Building 410  
Bolling AFB, Washington, DC 20332-6448

8a. NAME OF FUNDING / SPONSORING ORGANIZATION

8b. OFFICE SYMBOL  
(if applicable)

9. PROCUREMENT INSTRUMENT IDENTIFICATION NUMBER

AFOSR

NC

AFOSR-MIPR-86-00007  
AFOSR-MIPR-85-00002

8c. ADDRESS (City, State, and ZIP Code)

10. SOURCE OF FUNDING NUMBERS

Building 410  
Bolling AFB, Washington, DC 20332-6448

PROGRAM ELEMENT NO.	PROJECT NO.	TASK NO.	WORK UNIT ACCESSION NO.
61102F	4303	B1	

11. TITLE (Include Security Classification)

Product-state-resolved Kinetic Study of the  $H^+ + F^-$  Ion-ion Reaction (unclassified)

12. PERSONAL AUTHOR(S)

Dr. Hung-tai Wang

13a. TYPE OF REPORT  
Final

13b. TIME COVERED  
FROM 5-1-85 TO 4-30-86

14. DATE OF REPORT (Year, Month, Day)  
12-10-86

15. PAGE COUNT  
71

16. SUPPLEMENTARY NOTATION

None

17. COSATI CODES

FIELD	GROUP	SUB-GROUP

18. SUBJECT TERMS (Continue on reverse if necessary and identify by block number)

Ion-ion Recombination, Reactions,  
Nascent Population, Distribution,  
Binding, Energies of Negative Ions, ←

19. ABSTRACT (Continue on reverse if necessary and identify by block number)

This project was to investigate positive-ion/negative-ion recombination reactions. The achievements are listed in the following: 1) Detailed chemiluminescence spectra from ion-ion reactions were recorded. 2) Spectral analyses yielded reliable assignment of the product state. 3) Product-state-resolved nascent population distribution was obtained for the first time for an ion-ion reaction. 4) the product-state rotational population distributions are peaked at high J and the corresponding vibrational distribution favors only even numbered levels. And, 5) The investigation into the energy structure of negative ions yielded a revised Rydberg formula that proved to be a general formula for two-electron systems whose power and precision are equivalent to that of the original Rydberg formula for one-electron systems.

20. DISTRIBUTION / AVAILABILITY OF ABSTRACT

UNCLASSIFIED/UNLIMITED  SAME AS RPT.  DTIC USERS

21. ABSTRACT SECURITY CLASSIFICATION

unclassified

22a. NAME OF RESPONSIBLE INDIVIDUAL

Dr. Francis Wodarczyk

22b. TELEPHONE (Include Area Code)

(202) 767-4960

22c. OFFICE SYMBOL

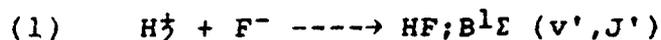
NC

1. SUMMARY OF ACHIEVEMENTS

The second year of this project was very fruitful. The fast-flow-reactor ensemble<sup>1</sup> was exploited to the fullest extent. The resultant kinetic and dynamic information on the  $H^+ + F^-$  and/or  $H_2^+ + F^-$  ion-ion reactions was likely the first of its kind. The paper on the nascent population distribution has been submitted to *Chem. Phys. Lett.*<sup>2</sup>. The effort on understanding the energy structure of negative ions has been very productive as well. Three papers resulted from this effort.<sup>3-5</sup>

1.1 ION-ION RECOMBINATION REACTION KINETICS AND DYNAMICS<sup>2</sup>

The product state of the reaction



was monitored *via* the chemiluminescence reaction



with  $h\nu$  in the 185-270 nm range. The observed transitions have  $0 < v' < 5$  and  $12 < v'' < 16$ .

All P- and R-branches show far-from-thermal rotational distributions that peak at high J levels. This indicates that the excess external angular momentum carried over the entrance channel is converted into internal rotational excitation in the exit channel.

There is a strong possibility that the  $v'$  population in the product state is concentrated in even-numbered vibrational levels. If true, this selectivity in the vibrational degree of freedom may need a novel mechanism for its rationalization.

<input checked="" type="checkbox"/>
<input type="checkbox"/>
<input type="checkbox"/>

Index

Dist	Special	or
A-1		

UNRECORDED

## 1.2 THE REVISED RYDBERG FORMULA FOR NEGATIVE IONS<sup>3-5</sup>

A Rydberg-like formula

$$(3) \quad T = -2R(Z-\sigma)^2 / (n^* + \mu)^2$$

was derived empirically. It proved to be very accurate in predicting electron affinities of a variety of negative-ion states that range from ground states to excited autoionization and/or resonance states. Its application spans both intra-atomic series and equivalent inter-atomic states. It is the most powerful and most accurate formula for describing the energy structure of both negative and positive ions available at present.

## 2. CONCLUSIONS

This project was perhaps the first probe into the realm of detailed kinetics of ion-ion reactions. The product state,  $\text{HF}; \text{B}^1\Sigma$ , is very likely the ideal system for state-to-state studies on such reactions. The present effort yielded some interesting results relating to the kinetics and the dynamics of those reactions. In order to investigate further into the mechanism of ion-ion reactions, a firmer knowledge on the internal properties of both positive and negative ions is imperative. The work on the energy structures of ions exemplifies an effort in that direction. The success of the revised Rydberg formula may have important implications beyond the realm of ion-ion reactions. It may significantly improve the fundamental understanding of electron correlation.

### 3. REFERENCES

- 1) "Product-state-resolved Kinetic Study of the  $H^+ + F^-$  Ion-ion Reaction", Hung-tai Wang, proposal to Air force Office of Scientific Research, 1983.
- 2) " $HF(B^1\Sigma \rightarrow X^1\Sigma)$  UV Chemiluminescence from the  $H^+/H_2^+ + F^-$  Ion-ion Reactions", Hung-tai Wang, *Chem. Phys. Lett.*, submitted.
- 3) "A Revised Rydberg Formula for Two-electron Systems. I.  $[\text{core}]ns^2$ ", Hung-tai Wang, *J. Phys. B: Atom. Molec. Phys*, 19 3401 (1986).
- 4) "A Revised Rydberg Formula for Two-electron Systems. II.  $[\text{core}]np^2$ ", Hung-tai Wang, *J. Chem. Phys*, 84 xx (1987).
- 5) "A Revised Rydberg Formula for Two-electron Systems. III. The  $ns^2$  Series of  $H^{**}$  and  $He^{**}$  and the He and C Isoelectronic Sequences", Hung-tai Wang, *Phys. Rev. A*, submitted.

#### 4. PREPRINTS

- 1) "HF( $B^1\Sigma \rightarrow X^1\Sigma$ ) UV Chemiluminescence from the  $H^+/H_2^+$  +  $F^-$  Ion-ion Reactions", Hung-tai Wang, Chem. Phys. Lett., submitted.
- 2) "A Revised Rydberg Formula for Two-electron Systems. II.  $(CORE)np^2$ ", Hung-tai Wang, J. Chem. Phys., 84 xxxx (1987).
- 3) "A Revised Rydberg Formula for Two-electron Systems. III. The  $ns^2$  Series of  $H^{-**}$  and  $He^{**}$  and the He and C Isoelectronic Sequences", Hung-tai Wang, Phys. Rev. A, submitted.

Submitted to  
Chem. Phys. Lett.

**HF( $B^1\Sigma \rightarrow X^1\Sigma$ ) UV CHEMILUMINESCENCE FROM THE  $H^+/H_2^+$  +  $F^-$  ION-ION  
REACTIONS**

Hung-tai Wang

Chemistry Division, Code 6180, Naval Research Laboratory,  
Washington, DC 20375-5000

ABSTRACT

Chemiluminescence spectra attributable to the  $H^+/H_2^+ + F^-$   $\rightarrow$  HF; $B^1\Sigma$  ion-ion reactions were obtained in the region between 185 and 270 nm. The rovibrationally resolved bands were assigned as HF; $B^1\Sigma(v', J')$  to HF; $X^1\Sigma(v'', J'')$  transitions with  $0 \leq v' \leq 4$  and  $12 \leq v'' \leq 16$ . The corresponding rotational branches all have peaks at high J values. These non-thermal distributions suggest that the corresponding product state  $v', J'$  populations reflect the nascent distribution from the ion-ion reactions.

## I. INTRODUCTION

Positive-ion/negative-ion (ion-ion) reactions have been extensively studied<sup>1</sup>. Most of the effort were to determine the overall reaction rates. Product-state-resolved (PSR) results are generally not available. Weiner, Peatman, and Berry<sup>2</sup> first reported Na D-line emission from the  $\text{Na}^+\text{O}^-$  ion-ion neutralization (NT) reaction. Smith, Adams, and Church<sup>3</sup> observed NO  $\gamma$ -band emission from the  $\text{NO}^+\text{NO}_2^-$  NT reaction. Apart from these, there is a scarcity of detail information on ion-ion reactions.

This lack of activity may be partly due to the usually inherent complications caused by curve crossings between the Coulomb potential and a number of neutral states. Even when the resultant chemiluminescence (CL) spectrum is simple, it is not always possible to assign its origin unambiguously<sup>3</sup>. Furthermore, there seems to be no PSR results on ion-ion recombination (RC) and ion-ion three-atom-exchange (TAE) reactions.

We have been studying the  $\text{H}^+\text{F}^-$  ion-ion NT/RC reactions and, as a by-product, the  $\text{H}_2^+\text{F}^-$  TAE reaction. Here, we would like to report some preliminary CL results. Our analysis indicates that a part of the non-thermalized nascent population distribution (NPD) of the product state might have been observed.

## II. BACKGROUND

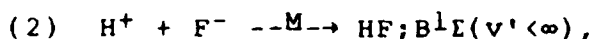
The common product state of the aforementioned NT, RC, and TAE reactions is the  $\text{HF};\text{B}^1\Sigma$  state. This state has several unique properties that make it an ideal product state for state-to-state studies on ion-ion reactions:

1) As shown in Figure 1, the  $B^1\Sigma$  is the lowest optically allowed excited bound state of HF. At  $R \sim 1 \text{ \AA}$  and  $E > 104,000 \text{ cm}^{-1}$ , the repulsive part of its potential intercepts some of the lowest Rydberg states with the  $HF^+; X^2\Pi$  core<sup>4</sup>. However, its attractive part is free from any curve crossing. The dissociative products of the B state are the ion pair  $[H^+; F^-]^4$ . Except the  $[H(n=2); F(^2P_{3/2})]$  neutral pair, all the other pairs with excited atomic H and/or F are at much higher energy. Most interestingly, the ionic and neutral pairs in the NT reaction

(1)  $H^+ + F^- \rightarrow H(n=2) + F(^2P_{3/2})$ ;  $-\Delta H < 0.07 \text{ kcal/mole}$ ,  
 are isoergic to each other to within  $-0.07 \text{ kcal/mole}$ , which is the experimental uncertainty of the electron affinity of the F atom ( $3.399 \pm 0.003 \text{ eV}$ )<sup>5</sup>. The binding energy of  $H(n=2)$  is  $3.3996 \text{ eV}$ <sup>6</sup>. The  $3 \text{ meV}$  upper limit of the energy gap between these two pairs can be translated into a curve crossing at  $R > 4800 \text{ \AA}$ .

2) Consequently, the B state can be termed a pure ionic state. As demonstrated in Table 1, the B curve follows the Coulomb potential to within 2% even at  $v'=4$ . This presents an opportunity for studying ion-ion NT/RC reactions without the complications caused by interferences from other nearby states.

The RC reaction



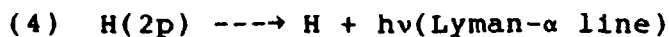
where M is a third body, can be studied directly. The B state can also be populated by the TAE reaction:



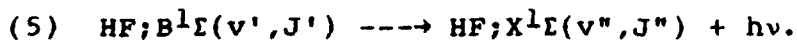
When the operational condition of the positive-ion source favors

the production of  $H_2^+$ , reaction (3) may dominate (2).

The above reactions can be monitored *via* CL observations of



and



Here, we report some CL results from reaction (5) in the 185-270 nm range.

### III. EXPERIMENT

Figure 2 is a schematic representation of the experimental facility. The main feature is a fast flow reactor with 1" ID pyrex tubing and a mechanical pump/Roots blower combination providing bulk flow velocity of ~80 m/sec. Negative and positive ions in He carrier gas, which was scrubbed by molecular sieve cooled in liquid  $N_2$ , are fed into the reactor separately. CL observation is made down stream from their mixing point. For the range of 185-270 nm, the spectra were measured with a Jarrell-Ash 1/4 meter spectrometer with 250  $\mu$  slit width at high blaze. Photon detection utilized SSR Quantum Photometer model 1140 and Pacific Photometric Instruments PMT model 3150, with the latter packed in dry ice. The scans reported here were recorded at 300 or 1000 counts/sec. The total pressure of a typical run is around 0.8 torr.

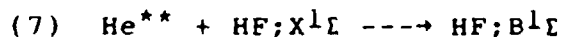
The ion sources were chosen for their simple designs. At the present exploratory stage of our study, both the quantities and the identities of the ions were not determined. The negative ion source was a microwave discharge flowing afterglow device.'

Fluorine was introduced into the He afterglow and  $F^-$  ions were generated by the dissociative-attachment reaction



The microwave power source operated at 2.45 GHz and 20 W. It was assumed that the negative ions were mostly  $F^-$  and, thus,  $F_2^-$  ions were ignored. The positive ion source was a He metastable generator modeled after the design of Richardson and Setser<sup>8</sup>. The electrodes were made of Tl and the typical discharge conditions were 350 V and 15 mA.  $H_2$  was fed into the  $He^{**}$  flow downstream and  $H^+/H_2^+$  ions were produced *via* Penning ionization. The ratio between  $H^+$  and  $H_2^+$  ions was likely  $<0.1^8$ . Other positive ions such as  $HeH^+$ ,  $HeH_2^+$ , and  $H_3^+$  might have also been produced. Although excluded in the current analysis, they could, if present in appreciable amounts, have significant contribution to the CL.

To certify the source of the CL, spectra were scanned under various flow conditions. All possible on/off combinations of the ion-source discharges and the flows of He,  $H_2$ , and  $F_2$  were tested. The flow rates of the three gases were adjusted until the right conditions for producing the  $HF(B \rightarrow X)$  CL emission and for suppressing spurious emissions from excited  $He_2$ ,  $H_2$ , and  $F_2$  were found. Flow reactors of different configurations with varying gas inlet positions relative to the discharges as well as the mixing point of the hydrogen and fluorine flows were constructed to determine the reproducibility of the CL. Furthermore, emission spectra from the reaction



were monitored and they proved to be quite different from those

attributed to the ion-ion reactions. These exercises, combined with the unambiguous assignments of the CL spectra as corresponding to the HF(B $\rightarrow$ X) transitions, led to the conclusion that the most plausible origin of the observed CL are the H<sup>+</sup>/H<sub>2</sub><sup>+</sup>+F<sup>-</sup> reactions.

A one-meter VUV spectrometer and a quadrupole mass spectrometer will be incorporated into the flow reactor to widen the range of CL observation and to increase the resolution as well as to eliminate the uncertainties in the ion contents of the ion sources. Overall reaction rates will be determined also.

#### IV. SPECTRAL ANALYSIS

Figures 3 and 4 show two CL spectra measured with different reactors under typical conditions described in the last section. The two reactors differ from each other in three aspects: the distance  $a$  in Figure 2 is twice as long for Figure 3 as for Figure 4,  $b$  for Figure 3 is fifteen times as long as for Figure 4, and,  $c$  for Figure 4 is one-tenth of that for Figure 3. Notice that, as a result of a shorter distance  $a$ , Figure 4 has higher overall intensity than 3. But, the shorter distance between the He<sup>\*\*</sup> generator and the observation window for 4 led to underlying diffuse bands that are attributed to He<sub>2</sub><sup>+</sup> emission.

Table 2 shows their vibrational analyses. Table 3 presents rovibrational assignments of the transitions in Figure 3. Molecular constants of and transition energies between the B and X states of HF are from Di Lonardo and Douglas<sup>4</sup>. The assignments are considered highly reliable due to the following reasons:

Firstly, the HF molecular constants and transition energies are unique among other possible candidates such as He<sub>2</sub>, H<sub>2</sub>, F<sub>2</sub>, etc. An extensive search failed to identify any alternative assignment that gave comparable rovibrational structures. Secondly, the agreement between observed HF CL rovibrational transitions and their literature values is within experimental uncertainties for most of the individual rotational states. And, thirdly, the rotational manifolds all show similar profiles which peak at high J values. Table 4 contains J" values corresponding to the maxima of each v'-v" band in Figure 3.

Extracted from the CL spectra in Figures 3 and 4, the relative populations of v' vibrational levels, with the v'=2 population normalized as 1, are in Table 5. The v'-v" transition dipole moments were calculated from the molecular constants' by using the program developed by Zare and Cashion<sup>9</sup> and they are presented in Table 2. The two population distributions are virtually identical except for the v'=3 level. Since the v'=3 band is missing in the higher intensity spectrum in Figure 4, the v'=3 assignment in the Figure 3 spectrum is not as reliable as the others.

#### V. DISCUSSION AND CONCLUSIONS

The radiative lifetimes of the v' levels converted from the computed transition moments are in the order of 10<sup>-8</sup> sec. At room temperature and 0.8 torr pressure, emission should be the major relaxation mechanism for the nascent population of v' levels generated by the ion-ion reactions. The lack of other means of relaxation is supported by the similarity between spectra A and B.

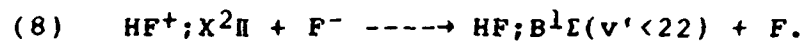
The origin of the nascent population, however, can not be

unequivocally determined. Assuming that the dominant positive ions are  $H^+$  and  $H_2^+$ , the two reactions in (2) and (3) can both populate the  $v'=0$  to 4 levels. Although the  $H_2^+/H^+$  ratio in the positive ion source is taken as  $>10$ , this dominance can be neutralized if the reaction rate of (2) is more than one order of magnitude faster than that of (3). Nonetheless, arguments can be made to support reaction (3) as the stronger candidate for producing the observed non-thermal population distribution. Any excess angular momentum carried by the heavier  $F^-$  ion in the entrance channel of reaction (3) is likely to remain within the  $HF;B$  molecule in the form of rotational excitation, since the departing H atom in the exit channel can carry only a small portion of the excess momentum in the form of translational energy. On the other hand, reaction (2) is a third-body reaction. The amount of rotational as well as vibrational radiationless relaxation depends on the collision partner, which is most likely He in this case. Without a third body, reaction (2) may produce  $HF;B$  molecule with very high  $v'$  and  $J'$ . In order to relax this nascent population with high  $v'$  and  $J'$  down to those in Tables 3 to 5, it would take multi-collisions between He atoms and a  $HF$  molecule in high  $v'$  and  $J'$ . This issue may be resolved by changing the collision partner and monitor the resultant CL.

If the uncertain  $v'=3$  assignment in Figure 3 is discounted, it is interesting to note that only even numbered  $v'$  levels are populated by the reactions. This selectivity in  $v'$  will be scrutinized further and, if substantiated, its implications will be explored. Note also that the two excited levels of  $v'=2$  and 4 account for  $>80\%$  of the total population at  $v'<5$ .

Because of the isolation of the B state from other states, few alternative reactions leading to this state are available.

One possible reaction is



But, it is considered less important since  $\text{HF}^+$  must first be produced by some secondary reactions.

Thus, it is concluded that the results described in Tables 3 to 5 may represent the nascent population distribution generated by the ion-ion reactions (2) and (3) in the range of 185-270 nm.

#### ACKNOWLEDGEMENT

This work was supported by the Air Force Office of Scientific Research under contract AFOSR-MIPR-85-0002.

## REFERENCES

- 1) D. Smith and N. G. Adams, *Physics of Ion-ion and Electron-ion Collisions*, Ed. F. Brouillard and J. W. McGowan, Plenum Press, New York, 1983, pp. 501-31, and references therein.
- 2) J. Weiner, W. B. Peatman, and R. S. Berry, *Phys. Rev. Lett.*, 25, 79 (1970) and *Phys. Rev. A*, 4 1824 (1971).
- 3) D. Smith, N. G. Adams, and M. J. Church, *J. Phys. B: Atom. Molec. Phys.*, 23 4041 (1978).
- 4) G. Di Lonardo and A. E. Douglas, *Can J. Phys.*, 51 434 (1973).
- 5) R. Milstein and R. S. Berry, *J. Chem. Phys.*, 55 4146 (1971).
- 6) C. E. Moore, *Atomic Energy Levels, National Bureau of Standards, USA, Circ. 467*, Vol. I, 1949.
- 7) A. L. Schmeltekopf, Jr. and H. P. Broida, *J. Chem. Phys.*, 39 1261 (1963).
- 8) W. C. Richardson and D. W. Setser, *J. Chem. Phys.*, 58 1809 (1973).
- 9) R. N. Zare and J. K. Cashion, University of California Radiation Laboratory, UCRL-10881, July 1963.

Table 1. Observed bonding energies' of the HF;B<sup>1</sup>Σ state are compared with E<sub>C</sub>, the Coulomb attraction energy of the [H<sup>+</sup>;F<sup>-</sup>] ion pair. R<sub>max</sub>'s are the outer turning points of the B state RKR potential'. E<sub>Obs</sub>'s are the differences between the B state dissociation limit and v' levels. ΔE=E<sub>C</sub>-E<sub>Obs</sub>. All energies are in cm<sup>-1</sup>.

v'	R <sub>max</sub>	E <sub>Obs</sub>	E <sub>C</sub>	ΔE	%
3	2.64	43030	43990	960	2.23
4	2.73	42006	42500	490	1.17
5	2.82	41013	41170	160	0.39
7	2.99	39275	38860	-420	-1.07
10	3.23	36477	35920	-560	-1.51
14	3.56	33306	32650	-660	-1.97
17	3.80	31159	30540	-620	-1.98
20	4.06	29190	28640	-550	-1.89
23	4.32	27382	26900	-480	-1.75
26	4.59	25725	25310	-417	-1.62

Table 2. Vibrational assignments for the bands in Figures 3 and 4 are given. All intensities, I (in arbitrary units), are normalized to the 2-12 band in Figure 3 by setting it to 1.0. Wavelengths,  $\lambda$  (in nm), are for the maxima of the vibrational bands. Transition dipole moments, D (in a.u.), are calculated from molecular constants<sup>a</sup> by using Zare and Cashion's program<sup>9</sup>.

$v' - v''$	Figure 3		Figure 4		$D_{v' - v''}$
	$\lambda$	I	$\lambda$	I	
4-12	198.7	0.13	198.7	0.65	1.76(-2)
3-12	203.1	0.10	--	--	7.20(-2)
2-12	209.3	1.0	209.5	3.3	1.10(-1)
2-13	220.7	0.91	220.5	2.4	7.80(-2)
2-14	230.5	0.46	230.6	0.80	7.00(-2)
0-14	241.6	0.29	241.2	0.34	2.09(-1)
0-15	253.0	0.67	252.2	1.6	3.18(-1)
0-16	265.1	0.71	265.7	1.0	2.66(-1)

Table 3. The spectrum in Figure 3 is rovibrationally analyzed. Rotational branches are designated as P(J'') and R(J''). I (in arbitrary units) is the intensity of individual rotational peaks. Experimental wavelengths,  $\lambda$  (in nm), are from Figure 3.  $E_{\text{obs}}$ 's are converted from  $\lambda$  and  $E_{\text{cal}}$ 's are calculated from molecular constants'.  $\Delta E = E_{\text{obs}} - E_{\text{cal}}$ . All energies are in  $\text{cm}^{-1}$ .

$\lambda$	I	$E_{\text{obs}}$	$v'-v'$	R(J'')	$E_{\text{cal}}$	$\Delta E$	P(J'')	$E_{\text{cal}}$	$\Delta E$
198.0	15	50500	4-12	R( 5)	50499	1	P( 4)	50501	0
198.3	14	50430		R( 6)	50410	20	P( 5)	50413	20
198.7	18	50330		R( 7)	50306	20	P( 6)	50308	20
199.0	17	50250		R( 8)	50187	60	P( 7)	50189	60
199.5	13	50120		R( 9)	50052	70	P( 8)	50054	70
200.1	10	49980		R(10)	49903	80	P( 9)	49905	80
201.4	7	49650	3-12	R( 3)	49605	50	P( 2)	49606	40
202.0	10	49500		R( 5)	49476	20	P( 4)	49477	20
202.7	14	49330		R( 6)	49388	-60	P( 5)	49389	-60
203.1	16	49240		R( 7)	49284	-40	P( 6)	49285	-40
203.5	11	49140		R( 8)	49165	-20	P( 7)	49166	-30
204.0	10	49020		R( 9)	49031	-10	P( 8)	49032	-10
204.4	7	48920	R(10)	48882	40	P( 9)	48882	40	
206.1	10	48520	2-12	R( 4)	48493	30	P( 4)	48494	30
206.5	13	48430		R( 5)	48420	10	P( 5)	48421	10
206.7	16	48380		--	--	--	--	--	--
206.9	18	48330		R( 6)	48333	0	P( 6)	48333	0
207.2	19	48260		R( 7)	48229	30	P( 7)	48230	30
207.8	51	48120		R( 8)	48111	10	P( 8)	48111	10
208.5	86	47960		R( 9)	47978	-20	P( 9)	47977	-10
209.0	104	47850		R(10)	47830	20	P(10)	47828	20
209.3	104	47780		--	--	--	--	--	--
210.0	64	47620		R(11)	47667	-50	P(11)	47665	-40
210.7	29	47460		R(12)	47492	-30	P(12)	47487	-30
211.3	13	47330		R(13)	47302	30	P(13)	47296	30
216.0	13	46300		2-13	R( 6)	46312	-10	P( 5)	46304
217.0	20	46080	R( 8)		46113	-30	P( 7)	46101	-20
217.4	17	46000	R( 9)		45993	10	P( 8)	45979	20
217.8	28	45910	--		--	--	--	--	--
218.2	27	45830	R(10)		45860	-30	P( 9)	45843	-10
218.9	30	45680	R(11)		45715	-40	P(10)	45695	-20
219.2	28	45620	R(12)		45557	60			
219.8	55	45500					P(11)	45535	-40
220.3	80	45390	R(13)		45388	0			
220.7	86	45310					P(12)	45362	-50
221.0	80	45250	R(14)		45207	40			
221.6	54	45130					P(13)	45178	-50
222.2	18	45000	R(15)		45016	-20	P(14)	44982	20
222.9	6	44860	--		--	--	--	--	--
223.2	6	44800	R(16)		44815	-20	P(15)	44776	20

Table 3. (continued, page 2 of 3)

$\lambda$	I	E <sub>obs</sub>	$v'-v'$	R(J <sup>m</sup> )	E <sub>cal</sub>	$\Delta E$	P(J <sup>m</sup> )	E <sub>cal</sub>	$\Delta E$	
227.5	5	43950	2-14	R(11)	43943	10				
228.0	8	43870					P(10)	43905	-30	
228.2	11	43820		R(12)	43805	20				
228.4	16	43780					P(11)	43762	20	
229.1	25	43650		R(13)	43657	-10				
229.5	35	43570					P(12)	43609	-40	
229.9	38	43490		R(14)	43500	-10				
230.2	44	43440					P(13)	43447	-10	
230.5	46	43390		R(15)	43334	60				
231.0	43	43300					P(14)	43275	20	
231.9	26	43130		R(16)	43160	-30	P(15)	43094	40	
232.6	10	43000		R(17)	42979	20				
233.4	9	42840		R(18)	42792	50				
239.6	10	41740		0-14	R(11)	41736	0			
240.0	16	41670						P(10)	41696	-30
240.4	21	41590			R(12)	41600	-10			
241.0	26	41500						P(11)	41554	-50
241.2	27	41460			R(13)	41454	10			
241.6	27	41390					P(12)	41402	-10	
242.5	17	41240					P(13)	41240	0	
243.0	14	41140	R(15)		41134	10				
243.4	9	41080					P(14)	41070	10	
244.0	6	40990	R(16)		40963	30				
245.9	8	40670	0-15		R( 5)	40660	10	P( 3)	40688	-20
246.3	8	40600			R( 6)	40601	0	P( 5)	40572	30
246.8	12	40520			R( 7)	40532	-10	P( 6)	40497	20
247.4	11	40420			R( 8)	40453	-30	P( 7)	40412	10
247.8	11	40360		R( 9)	40365	0				
248.1	13	40300					P( 8)	40317	-20	
248.4	18	40250		R(10)	40267	-20				
248.7	17	40210					P( 9)	40214	0	
249.1	15	40150		R(11)	40160	-10				
249.3	15	40110					P(10)	40100	10	
249.6	19	40060		R(12)	40046	10				
249.9	23	40020					P(11)	39978	40	
250.4	23	39930		R(13)	39923	10				
250.6	28	39900		--			--			
251.0	31	39840					P(12)	30848	-10	
251.5	39	39760		R(14)	39790	-30				
251.8	38	39710					P(13)	39710	0	
252.5	46	39610	R(15)	39659	-50					
252.8	54	39560				P(14)	39566	-10		
253.0	56	39530	R(16)	39518	10					
253.4	41	30470				P(15)	39415	50		
253.9	34	39380	R(17)	39373	10					

Table 3. (continued, page 3 of 3)

$\lambda$	I	E <sub>obs</sub>	$v'-v'$	R(J <sup>n</sup> )	E <sub>cal</sub>	$\Delta E$	P(J <sup>n</sup> )	E <sub>cal</sub>	$\Delta E$
259.2	13	38580	0-16	R(13)	38618	-40	P(11)	38620	-40
259.7	14	38510		R(14)	38519	-10	P(12)	38515	-10
259.9	16	38470		R(15)	38417	50	P(13)	38405	70
260.8	27	38340		R(16)	38312	30	P(14)	38291	50
261.6	22	38230		R(17)	38207	20			
261.8	19	38190					P(15)	38173	20
262.4	23	38120		R(18)	38103	20			
262.8	25	38050					P(16)	38054	0
263.0	27	38020		R(19)	38000	20			
263.4	27	37960					P(17)	37934	30
264.1	34	37860		R(20)	37903	-40			
264.7	44	37780		R(21)	37812	-30	P(18)	37815	40
265.1	55	37710		R(22)	37733	-20	P(19)	37698	10
265.5	54	37670		R(23)	37671	0			
266.2	43	37560					P(20)	37586	-30
266.8	32	37480					P(21)	37482	0
267.2	30	37420					P(22)	37389	30
267.7	18	37350					P(23)	37313	40

Table 4. These are the  $J'$  and  $J''$  values corresponding to the maximum (or maxima) for both the R- and P-branches in each vibrational bands in Figure 3.

$v - v''$	R-branch		P-branch	
	$J''$	$J'$	$J''$	$J'$
4-12	7	8	6	5
3-12	7	8	6	5
2-12	10	11	10	9
2-13	13	14	12	11
2-14	15	16	13	12
0-14	9	10	8	7
	13	14	12	11
0-15	10	11	9	8
	16	17	14	13
0-16	16	17	14	13
	22	23	19	18

Table 5. Relative nascent population distribution,  $N_{v'}$ , extracted from Figures 3 and 4 are listed. All  $v'$  populations are normalized to  $N_2'=1.00$ . Band intensities, transition energies, and transition dipole moments are from Table 2.

Relative Populations	$N_0$	$N_1$	$N_2$	$N_3$	$N_4$
Figure 3	0.26	0.00	1.00	0.14	0.70
Figure 4	0.18	0.00	1.00	0.00	0.68

## FIGURE CAPTIONS

Figure 1. Potential curves of HF are shown as functions of internuclear distance  $R$ . The  $X^1\Sigma$  curve and the  $v' < 27$  part of the  $B^1\Sigma$  curve are RKR potentials\*. The  $v' > 26$  part is extrapolated from the lower part by following the Coulomb curve.

Figure 2. A schematic diagram of the flow reactor is depicted. The notations  $a$ ,  $b$ , and  $c$  represent the distances between the merge point  $m$  and the optical window, between the  $H_2$  inlet and  $m$ , and between the  $F_2$  inlet and  $m$ , respectively.

Figure 3. This CL spectrum was measured with experimental conditions described in Section III. The reactor's dimensions as depicted in Figure 2 were  $a=40$  cm,  $b=45$  cm, and  $c=30$  cm. The count rate was 300 count/sec.

Figure 4. This CL spectrum was obtained with similar experimental conditions as in Figure 3. The reactor's dimensions were  $a=20$  cm,  $b=3$  cm, and  $c=3$  cm. The count rate was 1000 count/sec.

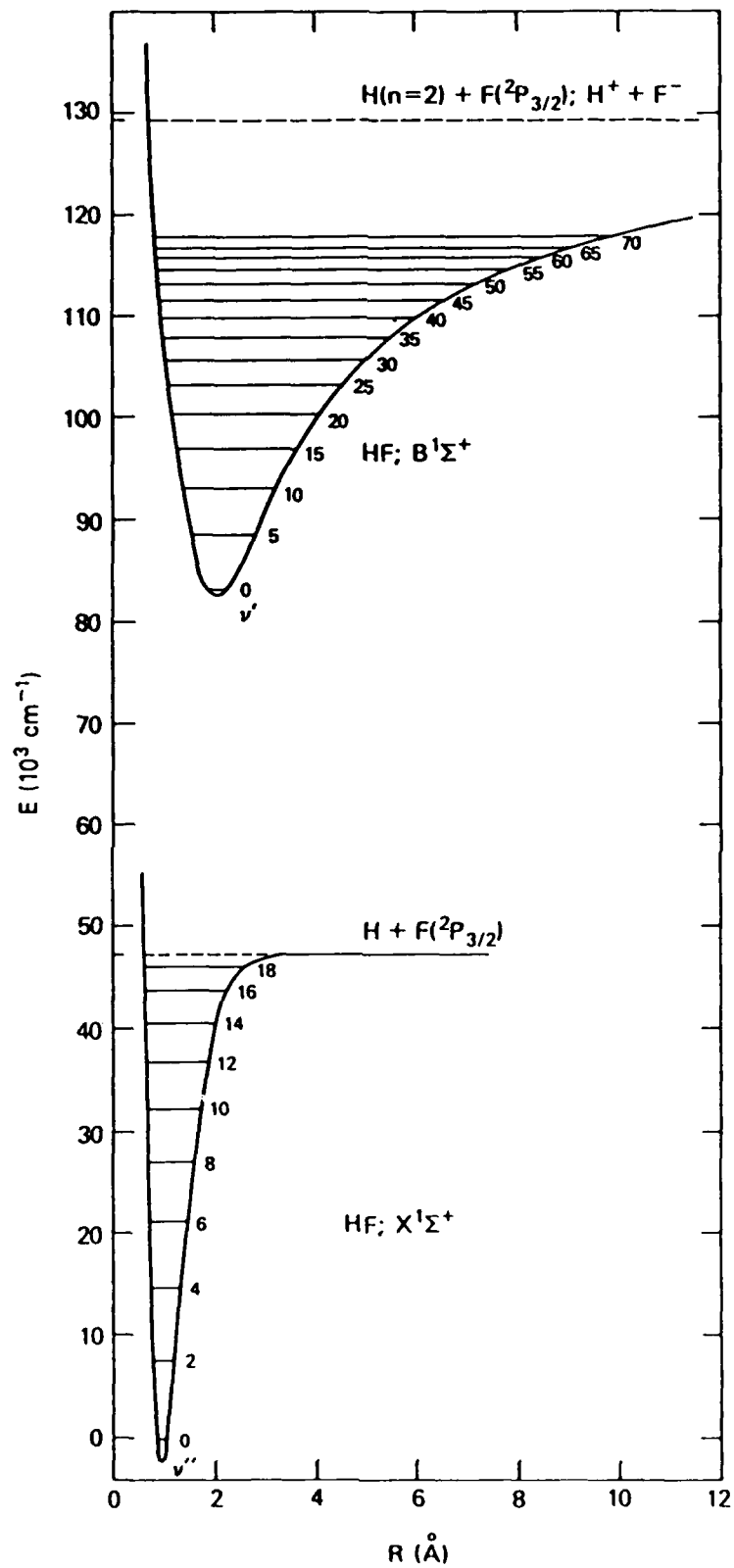


Figure 1

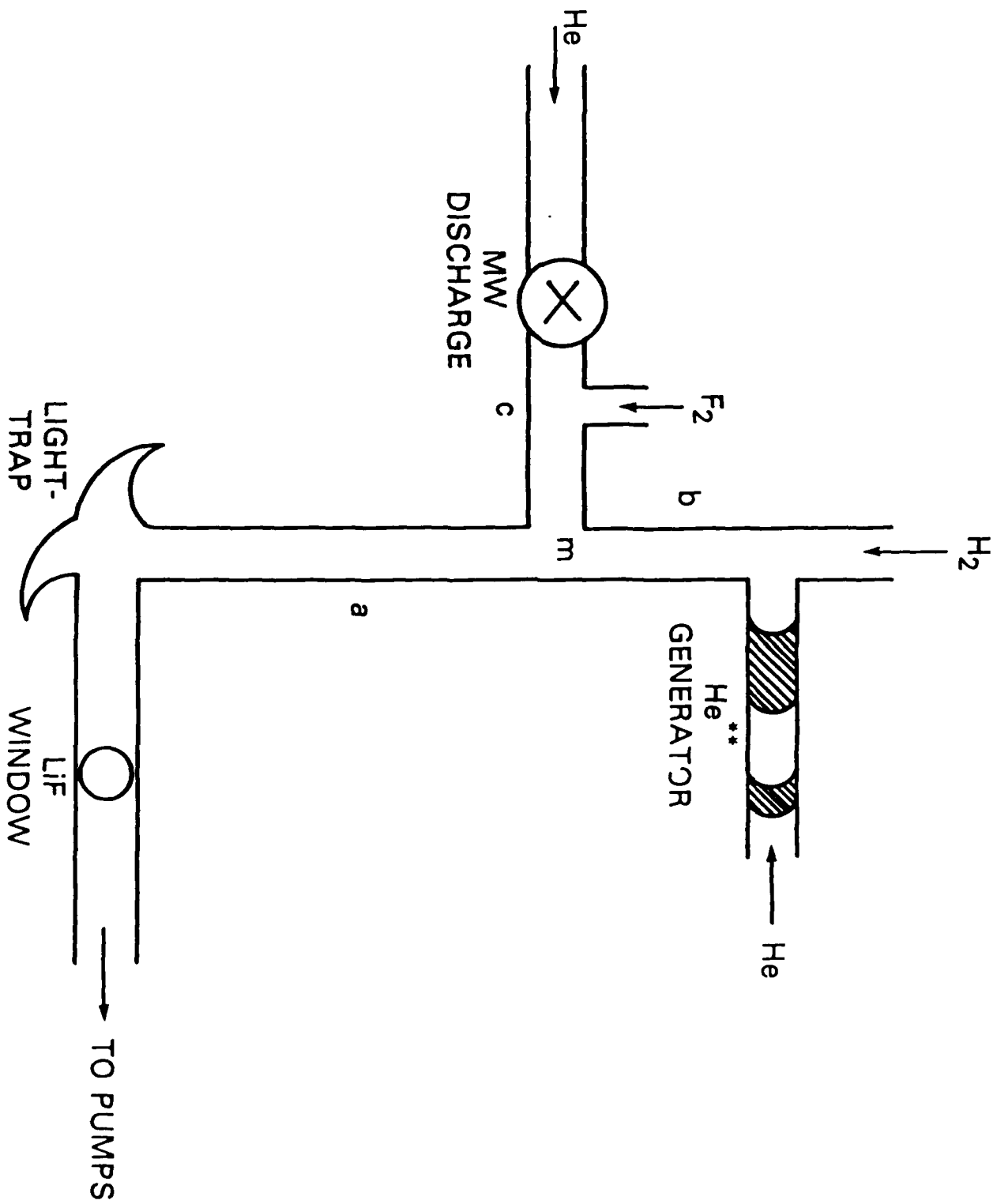


Figure 2

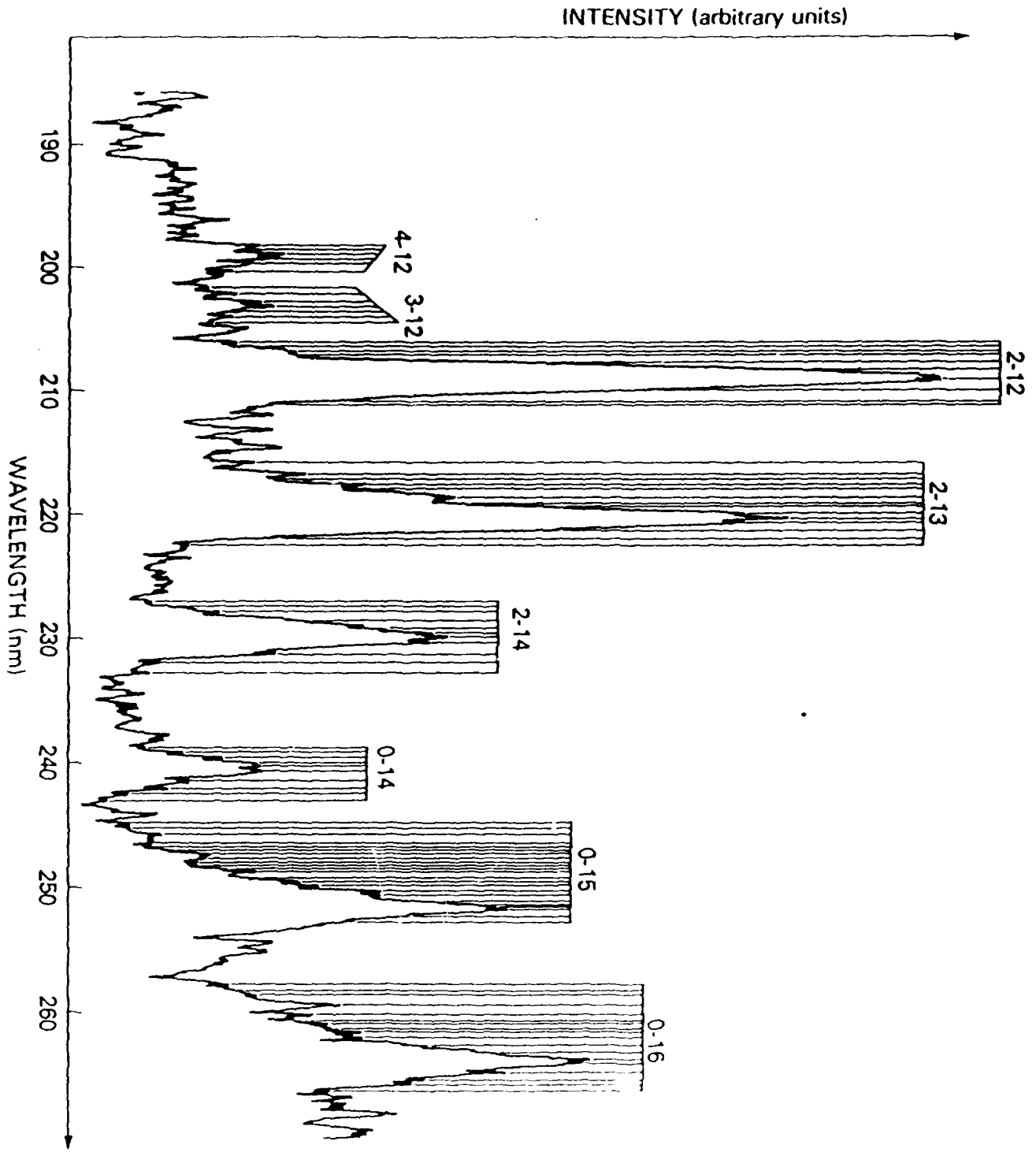


Figure 3

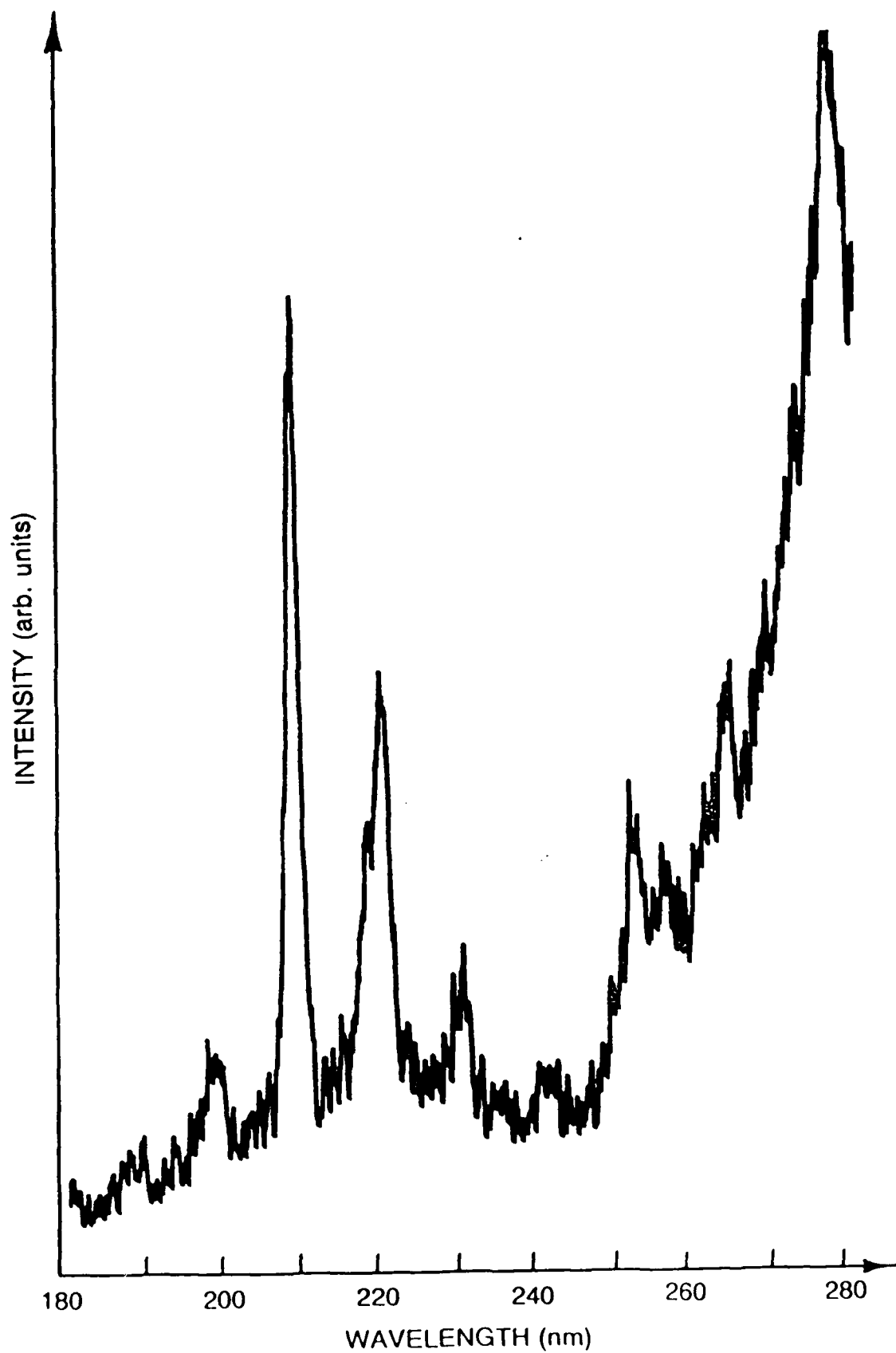


Figure 4

To appear in J. Chem. Phys  
in March 1987

A REVISED RYDBERG FORMULA FOR TWO-ELECTRON SYSTEMS. II. [CORE]np<sup>2</sup>

Hung-tai Wang<sup>a</sup>

Chemistry Division, Code 6180, Naval Research Laboratory,  
Washington, DC 20375

ABSTRACT

The revised Rydberg formula (RRF) described in paper I<sup>1</sup> for [core]n<sub>1</sub>l<sup>2</sup> two-electron systems with l=0 is extended here to l=1 cases. The two empirical parameters, the screening constant  $\sigma_l$  and a correction to the effective quantum number  $\mu_l$ , in the RRF have simple dependences on l, the core charge Z and core configurations. The accuracy of the RRF in calculating the two-electron binding energies of a variety of [core]np<sup>2</sup> species is demonstrated and the physical interpretations of  $\sigma_p$  and  $\mu_p$  and their relationships to  $\sigma_s$  and  $\mu_s$  are discussed.

## 1. INTRODUCTION

A revised Rydberg formula (RRF) for  $[\text{core}]n_{i\lambda}^2$  two-electron systems was derived empirically in paper I (P1) of this series'. It retains the simple form of the original Rydberg formula. The binding energy of the two  $n_{i\lambda}$  electrons to the core can be expressed as

$$(1) \quad T_{i\lambda}^2 = -2R(Z-\sigma_\lambda)^2 / (n_{i\lambda}^* + \mu_\lambda)^2,$$

where  $R$  is the Rydberg constant in  $\text{cm}^{-1}$ ,  $i$  is the degree of excitation,  $Z$  is the charge of the core,  $\sigma_\lambda$  is the screening constant,  $n_{i\lambda}^*$  is the effective quantum number (EQN) of the  $n_{i\lambda}$  electron in the  $[\text{core}]n_{i\lambda}$  one-electron system, and  $\mu_\lambda$  is the correction to the effective quantum number (CEQN) caused by the addition of the second  $n_{i\lambda}$  electron to form  $[\text{core}]n_{i\lambda}^2$ . The factor 2 accounts for the fact that each  $n_{i\lambda}$  electron experiences one-half of the two-electron binding energy,  $T_{i\lambda}^2$ .

For one-electron systems, the total charge is  $Z-1$ . For two-electron systems, it is  $Z-2$ . Thus, for  $[\text{core}]n_{i\lambda}^2$  systems,  $Z=1$  for negative ions,  $Z=2$  for neutral species, and  $Z=3, 4, \text{etc.}$  for positive ions. The highest *aufbau* principal quantum number in the core is  $n_0$ .

Figure 1 shows the relationship between the one-electron binding energy  $T_{i\lambda}$  and  $T_{i\lambda}^2$ . The former can be expressed via the conventional Rydberg formula as

$$(2) \quad T_{i\lambda} = -RZ^2 / (n_{i\lambda}^*)^2.$$

The quantum defect,

$$(3) \quad \delta_\lambda = n_i - n_{i\lambda}^*,$$

is a constant for a Rydberg series of  $[\text{core}]n_{i\lambda}$  states with fixed core configuration,  $\lambda$ , and  $Z$  but serial  $i$ 's.

P1 showed that the RRF's application encompasses most known  $[\text{core}]n_1s^2$  species from ground states to doubly-excited resonance or autoionization states with either closed-shell or open-shell cores. Unlike the Rydberg formula in Equation (2), which links an intra-atomic series of one-electron states by means of the constant  $\delta_l$ , the RRF is both intra-atomic and inter-atomic in nature. It's two empirical parameters  $\sigma_l$  and  $\mu_l$  can correlate not only intra-atomic series of two-electron states but also those belonging to different elements. Furthermore, through the  $Z$  dependence of  $\mu_l$ , it connects isoelectronic sequences ranging from negative ions to multiply charged positive ions. Consequently, the RRF has the potential to predict the binding energies of doubly-excited  $l=0$  states of most of the elements in the periodic table (and their isoelectronic sequences) with an accuracy comparable to current experimental uncertainties.

Similar revised Rydberg formulae were derived previously and they were reviewed in P1. Heddle<sup>2</sup> and Rau<sup>3</sup> both applied their formulae, which differ from Equation (1) mostly in that the EQN is replaced by the aufbau  $n_1$ , to intra-atomic series of species with three electrons or less. Read<sup>4</sup> did extensive inter-atomic studies with his formula, which can be obtained by letting  $\mu_l=0$  in Equation (1). All three formulae had varying degrees of success. However, the RRF in Equation (1) served to consolidate these efforts and provide concise and precise inter-atomic, intra-atomic and isoelectronic relationships.

The means of extracting the inter-atomic parameters  $\sigma_l$  and  $\mu_l$  from two-electron binding energies is the linear relationship established in P1,

$$(4) \quad M_{i\lambda} = an_{i\lambda}^* + b,$$

where  $M_{i\lambda}$  is converted from

$$(5) \quad T_{i\lambda}^2 = -2R/(M_{i\lambda}^2)$$

and the EQN from the one-electron binding energy *via* Equation (2).

Coupled with Equation (1), we have

$$(6) \quad Z_{\text{eff}} = Z - \sigma_{\lambda} = 1/a$$

and

$$(7) \quad \mu_{\lambda} = b/a = Z_{\text{eff}}b.$$

As demonstrated in Pl,  $a$  and  $b$  are constants for species with fixed  $i$  and  $Z$  but various core configurations. The resultant  $\sigma_S$  is independent of  $Z$  while the CEQN shows the isoelectronic behavior,

$$(8) \quad \begin{aligned} \mu_{\lambda} &= B_{\lambda}(1 - \sigma_{\lambda}) && ; Z=1 \\ &= (B_{\lambda}^{1+\alpha})/(Z^{1-\alpha}) && ; Z>1, \end{aligned}$$

with

$$(9) \quad \alpha = (10)^{\lambda-1} \sigma_{\lambda}.$$

The constant  $B$  is equal to  $b$  of  $Z=1$ . In Pl, for  $\lambda=0$ ,

$$(10) \quad \sigma_S = 0.225 \quad ; \quad B_S = 0.0865.$$

Notice that the behavior of the CEQN for  $Z=1$  negative ions differ from the  $Z>1$  cases. For negative ions, the CEQN is directly proportional to the screening constant, while, for neutral species and positive ions, it is scaled by a power of  $1/Z$ .

Pl also established that  $\sigma_S$  and  $\mu_S$  are invariant against different degrees of excitation  $i$ . Thus, they epitomize both the inter-atomic relationship among species with fixed  $i$  and  $Z$  but varying core configurations and the intra-atomic relationship among those with fixed  $Z$  and core configuration but changing  $i$ .

Unlike  $\lambda=0$  systems where the lowest value of the degree of

excitation is  $i=1$ , for  $\lambda=1$ , it could be either 0 or 1. For example, the species C I with electronic configuration  $[1s^2 2s^2] 2p^2$  and the species B\* with  $[1s^2 2s] 2p^2$  have the outermost s and p sharing the same *aufbau* principal quantum number  $n=2$ . Since  $n_0=2$  is the highest  $n$  in the core, 2p should correspond to  $i=0$  also. However, for the species Be\*\* with configuration  $[1s^2] 2p^2$ , 2p corresponds to  $i=1$  instead of 0. Thus,  $i=0$  may designate either the ground state or an excited state for a  $\lambda=1$  two-electron species, while  $i=1$  only indicates an excited state.

In this paper, Equations (1), (8), and (9) are tested for  $\lambda=1$  cases and the values of  $\sigma_p$  and  $\beta_p$  are obtained. However, due to the lack of data, the  $i>1$  intra-atomic relationship cannot be examined for  $\lambda=1$  systems as for  $\lambda=0$  species in Pl. Rather, only  $i=0$  or 1 inter-atomic relationships can be established. In addition, a comparative study is possible between  $[\text{core}]n_i p^2$  systems with closed-shell cores and those with cores that contain unfilled or half-filled s subshells. For each instance, an inter-atomic relationship characterized by the parameters  $\sigma_p$  and  $\beta_p$  can be obtained. The resultant RRF give very accurate  $T_{ip}^2$ 's. The physical interpretations of these inter-atomic relationships will be discussed and compared with the  $\lambda=0$  cases.

In order to simplify the notations, the following changes are made hereafter. Unless specified, all subscripts  $\lambda$  and  $i$  will be omitted. In addition,  $T=T_{ip}$  and  $T_2=T_{ip}^2$ .

## 2. INTER-ATOMIC RELATIONSHIP FOR $\lambda=1$ TWO-ELECTRON SYSTEMS

$[\text{core}]n_i p$  and  $[\text{core}]n_i p^2$  are both open-shell systems. To minimize effects caused by the split of the configurations, barycenters are used to establish the basis of the inter-atomic

relationship. But for the majority of  $\lambda=1$  two-electron systems of interest, not enough information is available to conduct the configuration averaging. In most cases, only a few energy levels of the split configurations are known. This prompted the attempt to apply the  $\lambda=1$  interatomic relationship obtained from the barycenters to situations where the known one- and two-electron energies are the lowest levels of the  $[\text{core}]n_1p$  and  $[\text{core}]n_1p^2$  configurations, respectively. As demonstrated below, similar relationships do exist for these split levels.

### 2.1 INTER-ATOMIC RELATIONSHIP FOR BARYCENTERS

Table 1 contains the species included in this  $\lambda=1$  correlative study. Barycenters of both their  $[\text{core}]n_0p$  and  $[\text{core}]n_0p^2$  configurations are available. They are isoelectronic to the carbon group elements and they serve as the prototype of  $\lambda=1$  two-electron systems with filled cores.

The number of members in each Z group does not warrant least-squares fitting. Instead, only the first two members of the Z=2 and 3 groups are featured in the extraction of the  $a$  and  $b$  parameters in Equation (4). As shown in Table 2, this lead to the following values *via* Equations (4) to (9):

$$(11) \quad a_p = 0.170 \quad ; \quad b_p = 0.2648.$$

These are inserted into Equations (8) and (9) to obtain the  $\mu_p$ 's for Z=3 groups. Coupled with Equation (11), these CEQN'S in column 6 of Table 2 allow the testing of the accuracy of the resultant  $\lambda=1$  RRF in Equation (1). As demonstrated in Table 3, the RRF can produce very accurate  $T_2$ 's for the species in Table 1. The overall average deviation is -0.07%, which is similar to that of the  $\lambda=0$  cases'.

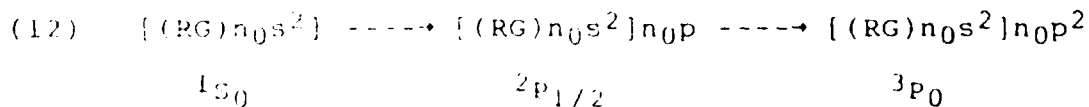
Thus, the applicability of the RRF in Equation (1) and the  $Z$  dependence of  $\mu$  in Equations (8) and (9) to  $l=1$  two-electron systems is established. Their applicability will be further extended to the lowest-energy split level of the  $[\text{core}]n_1p^2$  configuration in the following. This serves two purposes: First, since the lowest level is the experimentally most accessible, the impact of the RRF will be more significant. And, second, new insights into the physical interpretation of the RRF and its parameters  $\sigma$  and  $\mu$  can be gained from studying a more diversified group of  $l=1$  two-electron systems.

## 2.2 INTER-ATOMIC RELATIONSHIP FOR SPLIT LEVELS

Three groups of  $l=1$  two-electron systems will be studied in this section. The first is identified in Table 4 which consisted of the carbon group and their isoelectronic counterparts with totally filled cores. The second group have a half-filled  $s$  subshell in the core with the configuration of  $[(\text{RG})n_0s]n_0p^2$  where  $\text{RG}$  stands for the electronic configuration of the rare gas whose highest aufbau quantum number is  $n-1=n_0-1$  (add  $n-1d^{10}$  electrons for fourth to sixth row elements). They are shown in Table 5. The third group has an unfilled  $s$  subshell with the configuration  $[(\text{RG})]n_1p^2$  and they are collected in Table 6.

### 2.2.1 $[(\text{RG})n_0s^2]n_0p^2$ SPECIES

When the core is totally filled, the energy levels involved are:



For the species in Table 4, from their one- and two-electron binding energies, the following parameters are derived through

Equations (4) to (9):

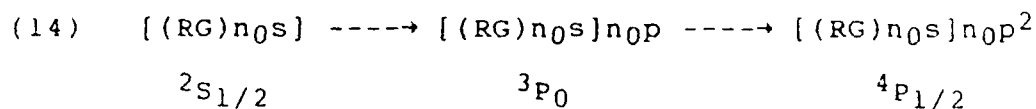
$$(13) \quad \sigma_p = 0.170 \quad ; \quad \beta_p = 0.238.$$

The data in Table 4 show that these parameters are capable of generating accurate  $T_2$ 's. Excluding the  $Z=1$  group, where the uncertainty in the electron affinities of Ga, In, and Tl are large, the overall average deviation is 0.2%. If only the species in Table 1 are included, the average deviation is 0.09%.

Therefore, a simple adjustment in the value of  $\beta$  is sufficient to treat individual split levels as successfully as configuration centers. This suggests that the screening constant is independent of spin-orbital couplings.

#### 2.2.2 $[(RG)n_0s]n_0p^2$ SPECIES

For cores containing a half-filled  $s$  subshell, the corresponding energy levels are:



Empirically fitted parameters have these values:

$$(15) \quad \sigma_p = 0.170 \quad ; \quad \beta_p = 0.263.$$

As evidenced by the data in Table 5, accuracy of the order of 0.1% can also be achieved for this group. The invariance of the screening constant against different coupling schemes again holds true. The value of  $\beta$  is only slightly different from the filled-core cases. This is remarkable considering the range of core configurations and core charges involved and the consequent variations in the nature of angular momentum couplings.

#### 2.2.3 $[(RG)]n_1p^2$ SPECIES

For the species in Table 6 with an unfilled  $s$  subshell in the core, the following energy levels are considered:

$$(16) \quad \begin{array}{ccc} [(\text{RG})] & \text{-----} & [(\text{RG})]n_1p & \text{-----} & [(\text{RG})]n_1p^2 \\ & & 1s_0 & & 2p_{1/2} & & 3p_0 \end{array}$$

The exercise of fitting experimental data to Equations (1), (8), and (9) yields

$$(17) \quad \sigma_p = 0.0833 \quad ; \quad \beta_p = 0.606.$$

However, this  $i=1$  group exhibits a different  $Z$  dependence of  $\mu$ . The exponent of  $Z$  in

$$(18) \quad \mu_i = (\beta_i^{1+\alpha}) / (Z^{1+\alpha}) \quad ; \quad Z > 1,$$

is  $1+\alpha$  instead of  $1-\alpha$  as in Equation (8). In other words,  $\mu$  can be expressed as

$$(19) \quad \mu_p = (\beta_p/Z)^{1+\alpha}.$$

But, as shown in Table 6, the agreement with experimental  $T_2$  deteriorate at high  $Z$ . Equation (19) underestimates  $\mu$  above  $Z=4$  systematically. This is manifested in the all positive  $\Delta T$  values. The large deviations for Ca I, Sr I, and Ba I could be due to some perturbation with nearby one-electron states. Excluding them, the overall average  $\Delta T$  is  $\sim 0.3\%$ .

This discrepancy notwithstanding, note that the  $i=1$  He\*\*  $2p^2; 3p_0$  energy level is very accurately calculated. By assuming that the  $Z=1$  negative ion portion of Equation (8) is still valid,  $\mu_p=0.556$  is used to compute the  $-T_2$  for the more interesting case of  $O^{+*} [1s^2 2s^2 2p^3] 3p^2$ , where the core is isoelectronic to nitrogen, the energy levels involved are:

$$(20) \quad \begin{array}{ccc} [N] & \text{-----} & [N]3p & \text{-----} & [N]3p^2 \\ & & 4s_{3/2} & & 3p_0 & & 3p \end{array}$$

The agreement with the observed value is within the experimental uncertainty. Hence, the same  $\mu=0.556$  and  $\sigma=0.0833$  are applied to

predict the  $-T_2$  for the  $H^{-**} 2p^2; ^3P_0$  energy level. The corresponding transition energy from the  $H; 1s$  ground state is 10.100 eV (1 eV=8065.479  $cm^{-1}$ ).

Therefore, an unfilled intracore s subshell with the same n as the two extracore np electrons changes the nature of the binding of the np electrons to the core. The change is reflected by the different values of  $\sigma$  and  $\mu$  and the different Z dependence of  $\mu$ . Moreover, the characteristics of this binding is independent of the contents of the inner shell(s) of the core, which ranges from a bare nucleus for the He isoelectronic  $2p^2$  species, to an open-shell [N] configuration for  $O^{-**}$ , and to totally filled  $n < n_0$  shells for the rest of the species in Table 6. In other words, all [core] $n_i p^2$  with  $i=1$  are related to each other in a fashion distinct from the  $i=0$  cases. The latter all share the same  $\sigma=0.170$  and have similar B's.

### 2.3 SUMMARY

The general form of the RRF applies to  $\lambda=1$  two-electron systems as well as to  $\lambda=0$  cases in Pl. The  $i=0$  screening constant  $\sigma_p=0.170$  is invariant to changes in the configuration and the angular momentum coupling schemes in the core when the core has either a closed-shell configuration or a half-filled valence shell s orbital. The corresponding  $\mu$ 's exhibit a Z dependence described by the same general formulae as in Pl. Additionally, their values are close to each other.

However, when the valence s subshell is unfilled, the  $i=1$  value of  $\sigma$  reduces to about one half of 0.170 while  $\mu$ 's more than double their values. At the same time, the Z dependence of  $\mu$  is changed from Equation (8) to Equation (19). Nonetheless, the

parameters in Equation (17) are able to correlate these  $i=1$  two-electron  $\lambda=1$  systems with a wide range of core configurations.

The interpretations of the above observations and their relevance to the  $\lambda=0$  inter-atomic correlations will be discussed in the next section.

### 3. DISCUSSION AND CONCLUSIONS

The empirical RRF has proved to be equally accurate for  $\lambda=1$  two-electron systems as for  $\lambda=0$  systems<sup>1</sup>. Its application requires only a knowledge of the one-electron binding energy  $-T$  and the pair of empirically fitted parameters  $\sigma$  and  $\mu$ . Through the inter-atomic (and intra-atomic for  $\lambda=0$ ) relationships and isoelectronic behaviors exhibited by these parameters, the RRF provides a unified treatment to a wide variety of  $[\text{core}]n_1\lambda^2$  systems that span: 1) the range of  $Z$  from negative ions to multiply charged positive ions, 2) various types of core configurations from bare nuclei to multilayered ones, 3) different degrees of excitation from ground states to excited resonance or autoionization states, and 4) both  $\lambda=0$  and  $\lambda=1$  species. Its simplicity, versatility, and accuracy make the RRF both an interesting subject for current theoretical investigations and a potentially powerful tool for experimental studies on two-electron systems.

#### 3.1 THE PROPERTIES OF $\sigma$

The screening constant is the fraction of  $Z$  shielded from the two electrons by each other and  $Z-\sigma$  is the effective core charge experienced by each electron. The binding of the two extra-core electrons is enhanced if they move in coordination such that  $\sigma$  is kept to a minimum. This correlated motion is important to the

stability of  $Z=1$  negative ions. As  $Z$  increases, it becomes less and less a factor. If an attempt is made to link  $\sigma$  to a degree of correlation between the two electrons, it should be guided by the following empirical observations:

- 1) Within an isoelectronic sequence, this degree of correlation remains the same as the core charge changes from  $Z=1$  for negative ions to  $Z>1$  for neutral species and positive ions.
- 2) With a fixed  $Z$ , the same degree of correlation exist for species with a wide range of core configurations.
- 3) For  $\lambda=0$ , both extra-core electrons are in the same  $s$  orbital. The amount of mutual screening is larger than the  $\lambda=1$  cases where the two electrons occupy two different  $p$  orbitals. This, however, could not lead to a direct comparison between the degrees of correlation associated with the  $\lambda=0$  and  $1$  two-electron systems.
- 4) For  $\lambda=0$ , the degree of correlation is independent of the degree of excitation<sup>1</sup>. Its equivalence can not be verified for  $\lambda=1$  due to the lack of  $i>1$  data.
- 5) For  $\lambda=1$ , the degree of correlation between the two extracore electrons increases from  $i=0$  intrashell to  $i=1$  extrashell cases as reflected by the decrease in  $\sigma$  from 0.179 to 0.0833. No analogy exists for  $\lambda=0$  systems because all extracore  $s$  orbitals are inevitably extrashell also.

### 3.2 THE PROPERTIES OF $\mu$

The following conclusions made in P1 are valid for  $\lambda=1$  also:  $\mu$  represents the increase in the orbital size associated with the addition of the second electron and the increase is confined to the extracore part of the orbital while the intracore part retains its original form. The constancy of  $\mu$  vs different core

configurations means that this increase in orbital size is independent of both the core and the original size of the  $n\lambda$  orbital in  $[\text{core}]n\lambda$ .

The  $Z$  dependence of  $\mu$  for  $\lambda=1$  share the same general formula in Equation (7) as  $\lambda=0$ . For  $Z=1$ ,  $\mu$  is directly proportional to  $\sigma$ . For  $Z>1$ , it is proportional to a power of  $Z$ . However, as reflected by the parameter  $\alpha$  in Equation (9), the exponent of  $Z$  deviate from  $-1$  much more for  $\lambda=1$  than for  $\lambda=0$ . This suggests that the interdependence between  $\mu$  and  $\sigma$  is stronger for  $\lambda=1$  than for  $\lambda=0$  two-electron systems with  $Z>1$ . Furthermore, the magnitude of the CEQN's for the  $\lambda=1$  cases with  $i=0$  are about three times as large as the  $\lambda=0$  cases. For  $i=1$ , they are about six times as large as the  $\lambda=0$  systems.

There is not enough information on the influence of innershell  $p$  precursors on the  $\lambda=1$  inter-atomic relationships to draw any conclusion. Nonetheless, it is interesting to note that the same set of  $\sigma$  and  $\mu$  governs the cases of  $\text{H}^{++}$  and  $\text{O}^{++}$ . It seems that the presence of  $2p$  precursors in the core of the latter has no effect.

In paper III of this series, the case of the He isoelectronic sequences with bare nuclei as the core will be examined together with the accuracy of the  $Z$  dependences of  $\mu$  for prototype  $\lambda=0$  and  $\lambda=1$  two-electron systems. Further empirical efforts may be worthwhile for  $[\text{core}]n_1\lambda_1 n_2\lambda_2$  systems with  $\lambda_1\neq\lambda_2$  and/or  $i\neq j$  as well as  $\lambda>1$ .

## ACKNOWLEDGEMENT

The encouragement and guidance of Professor R. Steven Berry is gratefully acknowledged. This work was sponsored by the Air Force Office of Scientific Research (AFOSR-MIPR-85-00002).

a) Earlier part of this work was done at Chemistry Department, The University of Chicago, Chicago, IL 60637.

## REFERENCES

- 1) Hung-tai Wang, *J.Phys.B:Atom.Molec.Phys.*, 1986, in press.
- 2) D. W. O. Heddle, *Electron and Photon Interactions with Atoms*, Ed. H. Kleinpoppen and M. R. C. McDowell, Plenum, New York, pp 671-8(1976).8
- 3) A. R. P. Rau, a) *J.Phys.B:Atom.Molec.Phys.*, 16 L699(1983)  
b) *Atomic Physics*, 9 491(1985).
- 4) F. H. Read, a) *J.Phys.B:Atom.Molec.Phys.*, 10 449(1977)  
b) *Aust.J.Phys.*, 35 475(1982).
- 5) C. E. Moore, *Ionization Potentials and Ionization Limits Derived from the Analysis of Optical Spectra*, NSRDS-NBS 34 (Washington, DC: US Government. Printing Office), 1970.
- 6) H. Hotop and W. C. Lineberger, *J.Phys.Chem.Ref.Data*, 4, 539(1975).
- 7) C. E. Moore, *Atomic Energy Levels, Circular 467*, (Washington, DC: US Government Printing Office),  
a) Vol. I, 1949.  
b) Vol. II, 1952.  
c) Vol. III, 1958.
- 8) W. C. Martin, *J. Phys.Chem.Ref.Data*, 2, 251(1973).
- 9) A. K. Edwards and D. C. Cunningham, *Phys.Rev.A*, 8, 158(1973)

Table 1. Species isoelectronic to the carbon group elements included in the  $\mu=1$  inter-atomic correlation study for barycenters are shown with their one-electron binding energies from Moore<sup>5</sup>. All energies are in  $\text{cm}^{-1}$ . The notation in parentheses represents only the electronic configuration of the designated element, not its nuclear configuration.

CONFIG.	(Be)2p <sup>2</sup>		(Mg)3p <sup>2</sup>		(Ca)4p <sup>2</sup>	
Z	SPECIES	-T <sub>0p</sub>	SPECIES	-T <sub>0p</sub>	SPECIES	-T <sub>0p</sub>
2	C I	196622.4	Si I	131646.8	Ge I	127343.1
3	N II	382588	P II	243000	As II	226710
4	O III	624126.5	S III	380907.9		
5	F IV	920930	Cl IV	546000		
6	Ne V	1272900	Ar V	732570		
7	Na VI	1680000				
8	Mg VII	2142500				

Table 2. Results of  $\sigma$  and  $\mu$  for the species in Table 1 are collected. Corresponding  $-T$ 's and  $-T_2$ 's are in Tables 1 and 3, respectively.

$Z$	$a$	$\sigma_p$	$b$	$\mu_p$	$\mu_p$
	<u>Equation (4)</u>		<u>Equation (4)</u>		<u>Eqs.(8)&amp;(11)</u>
2	0.5466	0.1705	0.06453	0.1181	0.1188
3	0.3533	0.1695	0.03011	0.0852	0.08488
4					0.06685
5					0.05555
6					0.04775
7					0.04201
8					0.03760

Table 3.  $-T_2^{\text{calc}}$ 's of the species in Table 1, calculated from Equations (1), (8), (9), and (11), are compared with the experimental  $-T_2$ 's. All  $-T$ 's and  $-T_2$ 's are from Moore<sup>s</sup>. The deviation is defined as  $\Delta T = -T_2^{\text{calc}} + T_2$  and  $\Delta T\% = 100|\Delta T/T_2|$ . The  $\mu$ 's for different Z groups are in Table 2. All energies are barycenters (in  $\text{cm}^{-1}$ ). The average of all  $\Delta T\%$  is 0.07.

<u>SPECIES</u>	Z	$-T_2$	$-T_2^{\text{calc}}$	$\Delta T$	$\Delta T\%$
C I	2	282626.6	282510	-120	0.04
Si I		194370.2	194320	-50	0.03
Ge I		188188.3	188350	160	0.08
N II	3	614116	614290	170	0.03
P II		397900	398280	380	0.09
As II		373030	372570	-460	0.12
O III	4	1057708	1058360	650	0.06
S III		656520	656950	430	0.06
F IV	5	1612000	1613240	1200	0.08
Cl IV		970920	970330	-590	0.06
Ne V	6	2277000	2278460	1500	0.06
Ar V		1330300	1328110	-2200	0.16
Na VI	7	3052400	3053810	1400	0.04
Mg VII	8	3934400	393420	1100	0.03

Table 4.  $-T_2^{\text{calc}}$  for  $[(RG)ngs^2]ngp^2$  systems calculated from Equations (1), (8), (9), and (13) are compared with  $-T_2$ , which, together with  $-T$ 's, are from Moore<sup>5</sup>. The values of  $\mu$  for each Z group are also shown. Electron affinities (EA) are from Hotop and Lineberger<sup>6</sup>.  $\Delta T$  and  $\Delta T\%$  are the same as in Table 3. All energies (in  $\text{cm}^{-1}$ ) are the lowest split level designated in Equation (12). Numbers in parentheses correspond to experimental uncertainties in the EA's.  $1 \text{ eV} = 8065.479 \text{ cm}^{-1}$ .

<u>SPECIES</u>	Z	$\mu$	$-T_2$	$-T_2^{\text{calc}}$	$\Delta T$	$\Delta T\%$
B <sup>-</sup>	1	0.198	69190	69210	20	0.03(0.12)
Al <sup>-</sup>			52000	52000	0	0.00(0.46)
Ga <sup>-</sup>			50800	52100	1300	2.56(2.38)
In <sup>-</sup>			49100	50460	1400	2.77(2.46)
Tl <sup>-</sup>			51700	52940	1200	2.40(3.12)
C I	2	0.105	287485.1	287510	30	0.01
Si I			197585.9	197410	-180	0.09
Ge I			192236	192700	460	0.24
Sn I			177248.8	177751	502	0.28
Pb I			181062	182350	1290	0.71
N II	3	0.0749	621454	621760	310	0.05
P II			402500	402700	200	0.09
As II			378960	379140	180	0.05
Sb II			337576	339950	2370	0.70
Bi II			340800	343000	2200	0.64
O III	4	0.0590	1067470	1068350	880	0.08
S III			662400	662640	200	0.03
Se III			594958	603080	8130	1.36
Te III			527300	527220	-80	0.01
F IV	5	0.0490	1624260	1625940	1680	0.10
Cl IV			978200	977600	-600	0.06
Br IV			863200	863000	-200	0.02
Ne V	6	0.0422	2291800	2294100	2300	0.10
Ar V			1339100	1337000	2100	0.16
Kr V			1155300	1156500	1200	0.10
Na VI	7	0.0371	3070000	3072800	2800	0.09
K VI			1754800	1750500	-4300	0.24
Rb VI			1481200	1481000	-100	0.01
Mg VII	8	0.0332	3959000	3962300	3300	0.08
Ca VII			2217600	2214400	-3200	0.14
Sr VII			1841900	1844300	2400	0.13
Al VIII	9	0.0301	4958800	4962600	3800	0.08
Sc VIII			2732000	2728500	-3500	0.13
Y VIII			2221000	2221700	720	0.03

Table 5.  $-T_2^{\text{calc}}$  for [(RG) $n_0s$ ] $n_0p^2$  species, calculated from Equations (1), (8), (9), and (15), are compared with  $-T_2$ .  $\Delta T$  and  $\Delta T\%$  are defined in Table 3. All energy levels are in  $\text{cm}^{-1}$ . Those designated in Equation (14) are from Moore'. Unavailable data are marked by (--). The overall average deviation is 0.31%. Excluding the sixth row elements Tl I, Pb II, and Bi III, the average deviation is 0.12.

SPECIES	Z	$\mu$	$-T_2$	$-T_2^{\text{calc}}$	$\Delta T$	$\Delta T\%$
B I	2	0.118	241010	241040	30	0.01
Al I			171118.4	170520	-600	0.35
Ga I			175874	175600	-270	0.16
In I			163887	164120	230	0.14
Tl I			168812	171710	2900	1.72
C II	3	0.0842	539905.5	540120	220	0.04
Si II			357897.4	358240	340	0.10
Ge II			352981.8	353160	180	0.05
Sn II			317572.8	318440	870	0.27
Pb II			320924	325980	5050	1.57
N III	4	0.0663	950378	950290	-90	0.01
P III			600800	599330	-1470	0.24
As III			--	569310	--	--
Sb III			506039	507120	1080	0.21
Bi III			501400	511880	10480	2.09
O IV	5	0.0551	1471864	1470380	-1480	0.10
S IV			895900	896190	300	0.03
F V	6	0.0474	2103020	2101410	-1610	0.08
Cl V			1243600	1242940	700	0.05
Ne VI	7	0.0417	--	--	--	--
Ar VI			1636770	1637890	1120	0.07
Na VII	8	0.0373	3696100	3692230	-4900	0.13
K VII			2083300	2085340	2000	0.10
Mg VIII	9	0.0338	4659300	4652790	6500	0.14
Ca VIII			2580300	2583700	3400	0.13
Al IX	10	0.0310	5731900	5724630	-7270	0.13
Sc IX			3128400	3132410	4000	0.13
Si X	11	0.0286	6915540	6906590	-8950	0.13
P XI	12	0.0266	8210300	8199340	-10960	0.13

Table 6.  $-T_2^{\text{calc}}$  for  $[(\text{RG})n]p^2$  species, calculated from Equations (1), (9), (17), and (19), are compared with  $-T_2$ .  $\Delta T$  and  $\Delta T\%$  are defined in Table 3. All energy levels are in  $\text{cm}^{-1}$ . Those designated in Equation (13) are from Moore<sup>1</sup>.  $-T$ 's for H He, and O are also from Moore<sup>1</sup>.  $-T_2$  for  $\text{He}^{**}; 2p^2(3P)$  is from Martin<sup>6</sup>. For  $\text{O}^{**}; [\text{N}]3p^2(3P)$ , where N stands for the ground state configuration  $1s^2 2s^2 2p^3; 4S_{3/2}$  of nitrogen, the  $-T_2$  is from Edwards and Cunningham<sup>9</sup>. Unavailable data are marked by (--). The overall average deviation is 0.50%.

SPECIES	Z	$\mu$	$-T_2$	$-T_2^{\text{calc}}$	$\Delta T$	$\Delta T\%$
$\text{H}^{**}; 2p^2$	1	0.556	--	28220	--	--
$\text{O}^{**}; [\text{N}]3p^2$			22970	23010	40	0.17
$\text{He}^{**}; 2p^2$	2	0.274	155918.1	155870	-48	0.03
Be I	2	0.274	162380.3	162370	-10	0.01
Mg I			125125.9	125090	-40	0.03
Ca I			106640.0	105200	-1440	1.35
Sr I			99702.5	98020	-1680	1.68
Ba I			88228.1	91430	3200	3.64
B II	3	0.177	409908.2	409620	-290	0.07
Al II			287221.6	287750	530	0.18
Ga II			298400	298000	-400	0.13
In II			276700	277300	600	0.22
Tl II			288000	288800	800	0.28
C III	4	0.130	769045.4	769010	-40	0.00
Si III			504617	506490	1870	0.37
Ge III			497046	497580	530	0.11
Sn III			447261.5	450680	3420	0.76
Pb III			456391	460960	4570	1.00
N IV	5	0.102	1238940	1239770	830	0.07
P IV			773837	778430	4590	0.59
As IV			729571	730610	1040	0.14
Sb IV			653400	661000	7600	1.17
Bi IV			650600	654400	3800	0.58
O V	6	0.0834	1819023	1821590	2570	0.14
S V			1096400	1102200	5800	0.53
Se V			998200	999400	1200	0.12
Te V			867600	875500	7900	0.92
F VI	7	0.0706	2509910	2514200	4290	0.17
Cl VI			1468700	1476900	8200	0.56
Br VI			1301700	1304700	3000	0.23
Ne VII	8	0.0611	--	--	--	--
Ar VII			1889980	1902400	12420	0.66
Na VIII	9	0.0538	4221800	4232100	10300	0.24
K VIII			2362500	2378000	15500	0.66
Mg IX	10	0.0480	5243400	5257700	14300	0.27
Ca IX			2885300	2903900	18600	0.64
Al X	11	0.0433	6376100	6394400	18300	0.29
Si XI	12	0.0394	7619200	7642400	23200	0.30
P XII	13	0.0361	8973700	9002500	28800	0.32

Figure 1. Energy levels of  $[\text{core}]n_1l^2$  systems. For  $Z=1$  cases, this diagram depicts a positive electron affinity.

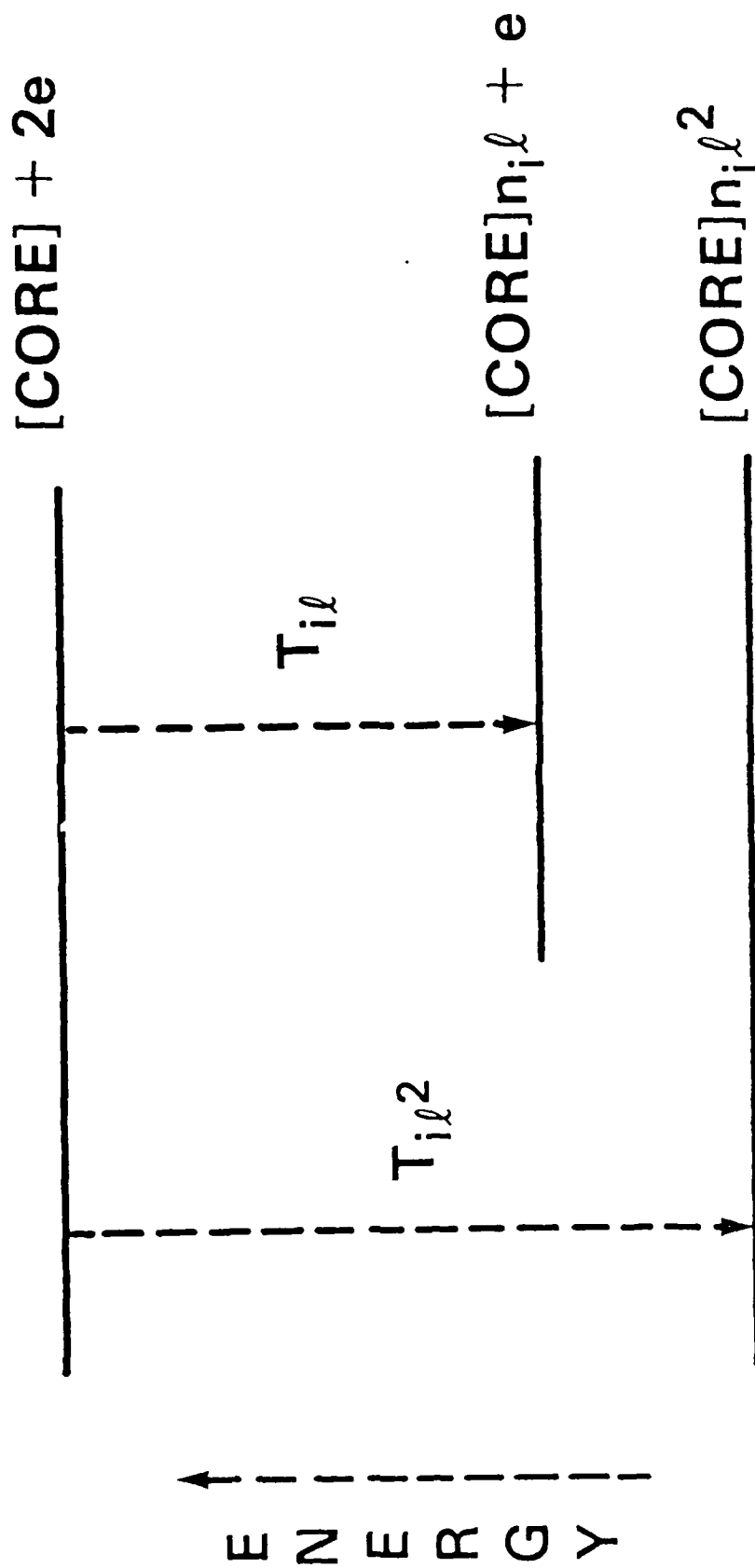


Figure 1

Submitted to  
Phys. Rev. A.

A REVISED RYDBERG FORMULA FOR TWO-ELECTRON SYSTEMS. III. THE  $ns^2$   
SERIES OF  $H^{-**}$  AND  $He^{**}$  AND THE He and C ISOELECTRONIC SEQUENCES

Hung-tai Wang

Chemistry Division, Code 6180, Naval Research Laboratory,  
Washington, DC 20375-5000

ABSTRACT

The revised Rydberg formula (RRF) for  $[\text{core}]n_l\lambda^2$  two-electron systems described in paper I<sup>1</sup> for  $\lambda=0$  and paper II<sup>2</sup> for  $\lambda=1$  is utilized here to study the  $n_l s^2$  intra-atomic series of  $H^-$  and He. In addition, the isoelectronic behaviors of the He and C sequences are also treated successfully by the RRF. The two-electron binding energies of the  $1s^2$  state of the He sequence with  $Z=1$  to 20 and the  $[1s^2 2s^2]2p^2$  state of the C sequence with  $Z=1$  to 14 are reproduced by the RRF with  $<0.05\%$  deviations. The properties of the resultant empirical parameters  $\sigma$  and  $\mu$  are interpreted and discussed in terms of inter-atomic and intra-atomic relationships as well as isoelectronic behaviors.

## 1. INTRODUCTION

A revised Rydberg formula (RRF) for  $[\text{core}]n_{i\lambda}^2$  two-electron systems was derived empirically in paper I<sup>1</sup> (P1) for  $\lambda=0$  and paper II<sup>2</sup> (P2) for  $\lambda=1$  species. The binding energy of the two  $n_{i\lambda}$  electrons to a core with charge  $Z$  is

$$(1) \quad T_{i\lambda}^2 = -2R(Z-\sigma_\lambda)^2 / (n_{i\lambda}^* + \mu_\lambda)^2.$$

It retained the simple form of the original one-electron Rydberg formula for the binding energy of one  $n_{i\lambda}$  electron to the same core:

$$(2) \quad T_{i\lambda} = -RZ^2 / (n_{i\lambda}^*)^2.$$

Figure 1 shows the relationship between  $T_{i\lambda}$  and  $T_{i\lambda}^2$ .  $R$  is the Rydberg constant in  $\text{cm}^{-1}$  and  $i$  is the degree of excitation.  $n_{i\lambda}$  is the effective quantum number (EQN) of the  $n_{i\lambda}$  electron in the one-electron system. While  $\sigma_\lambda$  is the screening constant,  $\mu_\lambda$  is the correction to the EQN (CEQN) caused by the addition of the second  $n_{i\lambda}$  electron. The factor 2 in Equation (1) accounts for the fact that each extracore electron in  $[\text{core}]n_{i\lambda}^2$  experiences one-half of the two-electron binding energy.

$Z=1$  for negative ions,  $Z=2$  for neutral species, and  $Z=3, 4, \text{etc.}$  for positive ions. The total charge of one-electron systems is  $Z-1$  and, of two-electron systems, it is  $Z-2$ . The highest Aufbau principal quantum number in the core is  $n_0$  and extracore orbitals are numbered as  $n_1, n_2, \text{etc.}$  accordingly.

Through its two parameters  $\sigma_\lambda$  and  $\mu_\lambda$ , as demonstrated in P1 and P2, the RRF yielded extensive inter-atomic as well as intra-atomic relationships that cover a wide range of two-electron systems. With the aid of the isoelectronic behavior of the CEQN,

$$(3) \mu_l = \beta_l(1-\sigma_l) \quad ; \quad Z=1$$

$$= (\beta^{l+\alpha})/(Z^{l-\alpha}) \quad ; \quad Z>1,$$

where  $\beta$  is a constant and

$$(4) \alpha = (10)^{l-1}\sigma_l,$$

the RRF is capable of calculating very accurate binding energies for a large number of two-electron systems, which span:

- A) The range of  $Z$  from 1 for negative ions to high  $Z$ 's for multicharged positive ions,
- B) Various types of core configurations from bare nuclei to multilayered ones,
- C) Different degrees of excitation from ground states to doubly-excited resonance or autoionization states, and
- D) Both  $l=0$  and  $l=1$ .

Similar formulae were derived by Heddle<sup>3</sup>, Read<sup>4</sup>, and Rau<sup>5</sup>. Heddle and Rau stayed with the conventional application of the Rydberg formula by studying intra-atomic series of doubly excited states. Both of their revised formulae have the basic form,

$$(5) T_{i,l,2} = -NR(Z-\sigma)^2/(n_{i,l}-\epsilon)^2,$$

with different factors  $N$  and different values of  $\sigma$  and  $\epsilon$ . They tested Equation (5) on systems with a total of three electrons or less:  $H^{-**}$ ,  $He^{**}$ , and  $He^{-**}$ . Read's formula,

$$(6) T_{i,l,2} = -2R(Z-\sigma)^2/(n_{i,l}^*)^2,$$

is equivalent to Equation (1) if  $\mu_l=0$ . Equation (6) was applied extensively by Read to  $l=0$  and 1 inter-atomic species.

Whereas both Equations (5) and (6) had varying degrees of success, the RRF in Equation (1) served to consolidate the task of revising the one-electron Rydberg formula for two-electron systems. Besides its potential for pinpointing binding energies

of unobserved two-electron systems, the RRF led to concise and precise inter-atomic, intra-atomic, and isoelectronic relationships that encompass a wide range of species. These empirical relationships suggest new approaches to studying electron correlation in two-electron systems.

The inter-atomic utilization of the RRF is reminiscent of the application of the original Rydberg formula in Equation (2) to correlate inter-atomic one-electron systems<sup>6</sup>. Some of the one-electron results will be published elsewhere<sup>7</sup>.

In this article, the RRF is applied to the special case of intra-atomic  $n_1s^2$  series of  $H^-$  and He whose cores are bare nuclei. The resultant  $\sigma_S$  and  $\mu_S$  are discussed and interpreted with reference to their counterparts obtained from systems with at least one electron in the core (P1). Also, the Z dependence of  $\mu_\lambda$  in Equations (3) and (4) are tested on the He; $1s^2$  isoelectronic sequence with Z=1 to 20 and the C; $[1s^22s^2]2p^2$  sequence with Z=1 to 14.

Unless necessary, the i and k subscripts will be omitted hereafter and  $T=T_{ik}$  while  $T_2=T_{ik}^2$ .

## 2. THE $n_1s^2$ SERIES OF $H^-$ AND He

The parameters  $\sigma$  and  $\mu$  for a group of related species can be extracted from their empirical binding energies via the linear relationship used extensively in P1 and P2:

$$(1) \quad M = \sigma n^2 + B,$$

where M is obtained from

$$(2) \quad T = -2R/M^2.$$

Comparing with Equation (1), we have

$$(9) \quad Z_{\text{eff}} = Z - \sigma = 1/a$$

and

$$(10) \quad \mu = b/a = Z_{\text{eff}}b.$$

Through linear-squares fitting, these Equations (7) to (10) yield the following for the  $n_i s^2$  series of  $H^-$  and He with  $i=1$  to 5:

$$(11) \quad \sigma = 0.174 \quad ; \quad \mu = 0.137 \quad \text{for} \quad Z=1 \\ = 0.0716 \quad \text{for} \quad Z=2.$$

Table 1 contains all the relevant data. High accuracy is maintained through  $i=1$  to 5 for both  $Z=1$  and 2. This establishes the intra-atomic relationship for  $ns^2$  systems for  $Z=1$  and 2.

This relationship describes the  $1s^2$  state with the same exactness as  $i>0$  doubly excited resonance and autoionization states. In P1, for the  $He^{-**}; [1s]ns^2$  series, the RRF gives binding energies for  $n=2$  to 8 states (except  $[1s]4s^2$ ) to within experimental uncertainties. Rau's Bohr-Rydberg formula<sup>5</sup> is only accurate for excited states. It produces larger deviations for  $i=1$  and/or 2 states than  $i>2$  states.

The implication of this RRF intra-atomic relationship that includes the  $i=1$  state could be significant. Assuming that the same  $\sigma=0.174$  holds for the  $n_i s^2$  series of  $Li^{+**}$ ,  $Be^{+**}$ , etc, their  $\mu$ 's can be obtained from the  $1s^2$  ground state binding energies of these positive ions and the  $T_2$ 's of all the  $ns^2$  series of the whole isoelectronic sequence can be calculated. These  $1s^2$  CEQN's are collected in Table 2 together with their corresponding experimental EQN's. From  $\mu=0.04741$  for  $Z=3$  and  $\mu=0.03538$  for  $Z=4$ , for instance, the  $2s^2$  doubly-excited autoionization state of  $Li^{+**}$  and  $Be^{+**}$  are predicted to have binding energies of -91.34 and -96.14 eV, respectively. The corresponding transition energies

from the  $1s^2$  ground state are 146.26 and 275.47 eV, respectively.

### 3. THE $1s^2$ ISOELECTRONIC SEQUENCE

From the empirical  $\mu$ 's shown in Table 2, the following isoelectronic relationship can be obtained for  $Z=1$  to 20:

$$(12) \quad \mu = B(1-\sigma) \quad ; \quad Z=1 \\ = B^{1.09}/Z \quad ; \quad Z>2$$

with

$$(13) \quad \sigma=0.174 \quad ; \quad B=0.166.$$

The constant  $B$  is the value of  $b$  for  $Z=1$ . The ability of Equation (12) in reproducing  $\mu$ 's is also shown in Table 2.  $T_2$ 's calculated from Equations (1), (12), and (13) are presented in Table 3. The overall average deviation from experimental  $T_2$ 's is 0.021%. Excluding the anomalous  $Z=2$  member, the average deviation is 0.014%.

On the other hand, the He; $1s^2$  isoelectronic species have been treated successfully by the inter-atomic relationship developed in P1 for  $[\text{core}]n1s^2$ . The  $i=1$  parameters in P1,

$$(14) \quad a = 0.225 \quad ; \quad b = 0.08623,$$

combined with the PRF and Equation (3) and (4), can also produce very accurate  $T_2$ 's for the same 20 isoelectronic species. With the exponents of  $B$  and  $Z$  in Equation (3) being 1.02 and 0.97, respectively, the computed  $\mu$ 's are compared with experimental ones in Table 4. The corresponding  $T_2$ 's are compared with the intra-atomic version in Table 3. For the inter-atomic cases, there is no anomaly at  $Z=2$  and the overall average deviation is 0.013%.

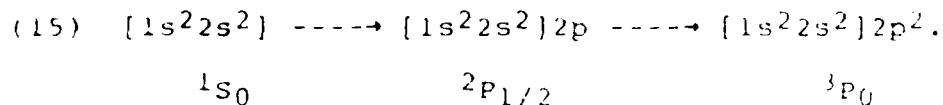
Therefore, the  $1s^2$  sequence can be described equally well by both the inter-atomic and the intra-atomic relationships. The

differences between the two approaches are in the values of  $\sigma$  and  $\beta$  and in the  $Z$  dependence of  $\mu$  as expressed by Equations (3) and (12). However, Equation (3) has an explicit  $\lambda$  dependence and it functioned well in P2 for  $\lambda=1$  systems. It's extension to high  $Z$  members of the C isoelectronic sequence will be examined in the next section.

#### 4. THE $[1s^2 2s^2] 2p^2$ ISOELECTRONIC SEQUENCE

The  $\lambda$  dependence in Equation (3) was established in P2 for  $[\text{core}]np^2$  systems with filled cores and with cores containing a half-filled  $s$  subshell. For the former, it is valid for both barycenters and split levels. Its applicability to high  $Z$  members of the C;  $[1s^2 2s^2] 2p^2$  sequence will be tested for the split levels in this section. The results for the  $Z=2$  to 8 members of the barycenters can be found in P2.

The energy levels involved are:



The parameters from P2 are:

$$(15) \quad \sigma_p = 0.170 \quad ; \quad \beta_p = 0.238,$$

and the exponents in Equation (3) are 1.17 for  $\beta$  and 0.82 for  $Z$ . The calculated  $T_2$ 's for  $Z=1$  to 14 are in Table 2. The average overall deviation from experimental values is 2.03%.

#### 5. SUMMARY

The RRF is applied to the intra atomic  $n_1^2$  series of H and He with high accuracy. The resultant parameters  $\sigma$  and  $\beta$  are different from the case whose core is not a rare member. These new parameters, however, led to an intra atomic isoelectronic

relationship for the He;1s<sup>2</sup> sequence in Equation (12) that is as powerful as the inter-atomic version in Equation (3). This suggests a dual quality for the members of this sequence. The implications of this duality will be discussed in Section 6.4. The  $\mu=1$  part of the inter-atomic isoelectronic relationship in Equation (3) proved to be just as accurate for the C;[1s<sup>2</sup>2s<sup>2</sup>]2p<sup>2</sup> sequence.

## 6. DISCUSSION AND RECAPITULATION

The RRF remained Rydberg-like. It is concise and precise. Its application to over 200 [core]n<sub>l</sub>l<sup>2</sup> two-electron systems with  $\mu=0$  and 1 is guided by a set of very simple inter-atomic and intra-atomic relationships complemented by isoelectronic behaviors. These systems cover the breadth of 1) a variety of core configurations from bare nuclei to multilayered cores with both closed- and open-shells, 2) different core charges ranging from Z=1 for negative ions to high Z's for multicharged positive ions, and 3) degrees of excitation from ground states to highly doubly-excited states. The overall average deviation between the calculated two-electron binding energies and the literature values is 0.3%. The actual accuracy of the RRF could be around 0.1% since most of the larger deviations are very likely due to experimental uncertainties.

### 6.1 THE Z dependencies of $\sigma$ AND $\mu$

The isoelectronic behaviors of the two parameters  $\sigma$  and  $\mu$  in the RRF are: First, the screening constant  $\sigma$  is independent of Z in all cases studied. Second, for Z=1 negative ions,  $\mu=8(1-\sigma)$  is true for all two-electron systems investigated. And, third, for neutral species and positive ions, the Z dependence of  $\mu$  has three

basic forms:

A) The inter-atomic relationship of the He;1s<sup>2</sup> sequence shares

$$(3) \quad \mu = (\beta^{1+\alpha}) / (Z^{1-\alpha}) \quad ; \quad Z > 1$$

with all the other  $\mu=0$  species in P1 as well as the the  $i=0$  species with  $\mu=1$  in P2.

B) For  $\mu=0$  species with bare-nucleus cores; *i. e.*, ns<sup>2</sup> species isoelectronic to He, the intra-atomic relationship requires the Z dependence in

$$(12) \quad \mu = \beta^{1.09/Z} \quad ; \quad Z > 1,$$

which has no explicit involvement of  $\alpha$ .

C) The  $i=1$  species with  $\mu=1$  in P2 exhibit that

$$(17) \quad \mu = (\beta/Z)^{1+\alpha} \quad ; \quad Z > 1,$$

with

$$(18) \quad \sigma = 0.0833 \quad ; \quad \beta = 0.606.$$

The parameter  $\alpha$  is defined in Equation (4). Note that the exponent of Z in the three equations range from  $1-\alpha$  in (3), to 1 in (12), and to  $1+\alpha$  in (17). Also,  $\beta$  in Equations (3) and (17) has powers of  $1+\alpha$  while, in Equation (12), there is no apparent connection between  $\alpha$  and the exponent of  $\beta$ .

## 6.2 INTRA-ATOMIC RELATIONSHIPS

Intra-atomic relationships link states with the same core configuration, a fixed Z, and identical  $\mu$  but a changing serial  $i$ . Data for such series of doubly-excited states are scarce. The three examples available are the He<sup>-\*\*</sup>;{1s|n<sub>1</sub>s<sup>2</sup> series with  $i=1$  to 7 by Buckman *et al*<sup>12</sup> discussed in P1 and the n<sub>1</sub>s<sup>2</sup> series of H<sup>-</sup> and He described in the present article. For He<sup>-\*\*</sup> in P1,

$$(19) \quad \sigma = 0.214 \quad ; \quad \beta = 0.0865.$$

For  $H^-$  and He,

$$(13) \quad \sigma = 0.174 \quad ; \quad \beta = 0.166.$$

Comparing with

$$(14) \quad \sigma = 0.225 \quad ; \quad \beta = 0.08623,$$

it is clear that, although there are three distinct values of  $\sigma$  for  $\lambda=0$  systems, there are only two values of  $\beta$  with one being nearly one half of the other.

In P1, it was postulated that Equation (14) represents the intra-atomic relationship for all  $\lambda=0$  two-electron systems other than the He sequence and those with a half-filled s subshell in the core. And, furthermore, those with a half-filled subshell all conform to Equation (19). If both postulations are true, for a fixed Z, the linear relationship in Equation (7) yields three straight lines in a plot of M vs  $n^*$  with slopes  $a=1/(Z-\sigma)$  and intercepts  $b=\mu/(Z-\sigma)$ . These three lines then contains all the intra-atomic series of ground as well as doubly-excited states of  $\lambda=0$  two-electron systems with core charge Z.

The He-sequence line with  $\sigma=0.174$  crosses the  $\sigma=0.225$  line at the point of  $n^*=1$  and the  $\sigma=0.214$  He<sup>-\*\*</sup> line meets the  $\sigma=0.225$  line at the  $n^*=0$  point. The  $n^*=1$  point is the  $1s^2$  species while the  $n^*=0$  point corresponds to merging the core electrons into the nucleus followed by collapsing the two extra-core s electrons toward this new nucleus.

The Z dependence of the  $\sigma=0.225$  and 0.214 lines is described by Equation (3), whereas of the  $\sigma=0.174$  line, it is depicted by Equation (17).

### 6.3 INTER ATOMIC RELATIONSHIPS

Inter-atomic relationships associate states with the same  $l$ ,

a fixed  $Z$ , and identical  $\lambda$  but varying core configurations. For  $\lambda=0$  and  $i=1$ , Equation (14), coupled with Equations (3) and (4), embodies the inter-atomic relationship. For  $\lambda=1$  and  $i=0$ , Equation (16), together with Equations (3) and (4), represents the relationship. The presence of a half-filled  $s$  subshell in the core for  $\lambda=1$  cases does not appreciably alter the inter-atomic relationship (P2). However, for  $\lambda=1$  and  $i=1$ , Equations (17) and (18) provide the connection.

Note that the  $\sigma$  in Equation (18) is about one-half of that in Equation (16). It is possible that the combination in Equation (18) also serves as the intra-atomic relationship for  $i>1$  and  $\lambda=1$  two-electron systems. In P2, Equations (17) and (18) were shown to be able to successfully deal with the  $2p^2$  autoionization state of  $\text{He}^{**}$  and the  $[1s^2 2s^2 2p^3] 3p^2$  resonance state of  $\text{O}^{-**}$ . Unfortunately, there is no data for a  $\lambda=1$  series with higher  $i$ 's to confirm this speculation.

#### 6.4 THE DUALITY OF THE $\text{He}; 1s^2$ ISOELECTRONIC SEQUENCE

As mentioned in Section 6.2, in a  $M$  vs  $n^*$  plot for a certain  $Z$ , the  $\sigma=0.225$  line and the intra-atomic  $\sigma=0.174$  line converge on the  $1s^2$  point. In addition, the  $1s^2$  isoelectronic sequence has been treated with similar accuracies by the two distinct isoelectronic relationships in Equations (3) and (12). This suggests that the  $1s^2$  point is on the joint boundary of two potential energy surfaces mapping the  $\sigma=0.225$  (S1) and the  $\sigma=0.174$  (S2) relationships. Away from the  $1s^2$  position, the gap between S1 and S2 is caused by the presence or the absence of the quantum defect  $\delta$  defined in

$$(20) \quad n^* = n - \delta.$$

Since S2 corresponds to systems with bare-nucleus cores, it is characterized by  $\delta=0$ . S1 is therefore for all  $\delta \neq 0$  species, with the exception of the half-filled s subshell systems, which follows the third  $\sigma=0.214$  surface (S3) that intercepts the  $\sigma=0.225$  one at  $-T_2 \rightarrow \infty$ . It should be pointed out that, while S2 and S3 are manifestly independent of the degree of excitation  $l$ , this independence is only assumed for S1.

However, at  $n^*=1$ , both mechanisms associated with S1 and S2 seem to be operative. One added clue to this problem could be in the different isoelectronic behaviors of the He;ls<sup>2</sup> sequence as described in Equations (3) and (12). For Z=1 negative ions, S1 and S2 have the same dependence on the screening constant  $\sigma$ . For neutral species and positive ions, S1 and S2 differ in the exponents of both  $\beta$  and Z. The power of  $\beta$  is  $1+\alpha$  for S1 and 1.09 for S2. Those of Z are  $1-\alpha$  and 1 for S1 and S2, respectively. Thus, for Z>1, the CEQN of S1 is interdependent on the screening constant  $\sigma$  through  $\alpha$ , while there is no apparent connection between  $\mu$  and  $\sigma$  for S2.

Assuming that, with suitable representation, the correlation between the two ns electrons could be categorized into terms containing either  $\mu$  or  $\sigma$ . Then, for Z>1, the S2 potential surface would be separable in terms of  $\mu$  and  $\sigma$ . This separability would not apply to S1. Moreover, for Z=1, both S1 and S2 would share the same expression with different values of  $\sigma$  and  $\mu$ .

## 7. CONCLUSIONS

The PRF in Equation (1) can be regarded as the two-electron equivalent of the original one-electron Rydberg formula in

Equation (2). In addition to its ability to describe intra-atomic series similar to the conventional application of Equation (2), the RRF has also provided extensive inter-atomic relationships and isoelectronic behaviors. Experimentally, it could be a powerful tool in predicting energy positions of new two-electron states. Theoretically, it offers new approaches to study the properties of two-electron systems in general and of doubly-excited states in particular. It may be worthwhile to further pursue the empirical exploration into  $[\text{core}]n_1l^2$  two-electron systems with  $l > 1$  as well as  $[\text{core}]n_1l n_1l'$  with  $l \neq l'$ .

#### ACKNOWLEDGEMENT

The sponsorship of the Air Force Office of Scientific Research (AFOSR-MIPR-85-00002) is acknowledged.

## REFERENCES

- 1) H-t. Wang, *J. Phys. B: Atom. Molec. Phys.*, in press.
- 2) H-t. Wang, *J. Chem. Phys.*, submitted.
- 3) D. W. O. Heddle, *Electron and Photon Interaction with Atoms*, Ed. H. Kleinpoppen and M. R. C. McDowell, Plenum, New York, pp. 671-8 (1976).
- 4) F. H. Read, a) *J. Phys. B: Atom. Molec. Phys.*, 10 449 (1977)  
b) *Aust. J. Phys.*, 35 475 (1982).
- 5) A. R. P. Rau, a) *J. Phys. B: Atom. Molec. Phys.*, 16 L699 (1983).  
b) *At. Phys.*, 9 491 (1985).
- 6) H-t. Wang, *PhD dissertation*, Louisiana State University, 1976.
- 7) H-t. Wang, manuscript in preparation.
- 8) C. E. Moore, a) *Atomic Energy Levels, Circular 467, Vol. I*, Washington DC: US Government Printing Office, 1949.  
b) *Atomic Energy Levels, Circular 467, Vol. II*, 1952.  
c) *Atomic Energy Levels, Circular 467, Vol. III*, 1958.  
d) *Ionization Potentials and Ionization limits Derived from the Analysis of Optical Spectra*, NSRDS-NBS 34, Washington DC: US Government Printing Office, 1970.
- 9) H. Hotop and W. C. Lineberger, *J. Phys. Chem. Ref. Data*, 4 539 (1975).
- 10) J. F. Williams, *Electron and Photon Interactions with Atoms*, Ed. H. Kleinpoppen and M. R. C. McDowell, Plenum, New York, pp. 309-39 (1976).
- 11) W. C. Martin, *J. Phys. Chem. Ref. Data*, 2 257 (1973).
- 12) S. J. Buckman, P. Hammond, F. H. Read, and G. C. King, *J. Phys. B: Atom. Phys. Molec. Phys.*, 16 4039 (1983).

Table 1.  $-T_2$ 's computed from Equations (1) and (11) for  $n1s^2$  series of  $H^-$  and He are compared with literature values  $-T_L$ . All the one-electron  $-T$ 's and  $-T_L$  for  $He;1s^2$  are from Moore<sup>8</sup>. Electron affinity of H is from Hotop and Lineberger<sup>9</sup>. For  $2s^2$ , the  $-T_L$  for  $H^-$  is from Williams<sup>10</sup> and for He from Martin<sup>11</sup>. The rest of the  $-T_L$ 's are from Rau<sup>5</sup>. Numbers in parentheses are experimental uncertainties. All energies are in eV.  $\Delta T = -T_2 + T_L$ . (1 eV = 8065.479  $cm^{-1}$ ).

Z	Conf.	$-T_L$	M	$n^*$	$-T_2$	$\Delta T$
1	$1s^2$	14.3529	1.37651	1.0000	14.354	0.001
	$2s^2$	4.042(10)	2.587	2.0000	4.063	0.021
	$3s^2$	1.886	3.798	3.0000	1.886	0
	$4s^2$	1.085	5.008	4.0000	1.084	-0.001
	$5s^2$	0.704	6.219	5.0000	0.703	-0.001
2	$1s^2$	79.0058	0.58684	1.0000	79.004	-0.002
	$2s^2$	21.136(40)	1.134	1.9998	21.143	0.007
	$3s^2$	9.61	1.682	2.9994	9.619	0.01
	$4s^2$	5.49	2.229	3.9986	5.476	-0.01
	$5s^2$	3.54	2.776	4.9972	3.531	-0.01

Table 2.  $\mu^*$ 's for the  $1s^2$  state with  $Z=1$  to 20 are converted from Equation (1) by using  $\sigma=0.174$  and the experimental  $-T_2$ 's in Table 3. EQN's are from  $1s$  binding energies in Moore<sup>8</sup>.  $\mu$ 's are calculated from Equation (12) with  $\sigma=0.174$  and  $\beta=0.166$ .  $\Delta\mu=\mu-\mu^*$ .  $\Delta\mu\% = 100|\Delta\mu/\mu^*|$ .

Z	SPECIES	EQN	$\mu^*$	$\mu$	$\Delta\mu$	$\Delta\mu\%$
1	H <sup>-</sup>	0.99999	0.1370	0.1371	0.0001	0.07
2	He I	0.99998	0.07159	0.07061	-0.00098	1.37
3	Li II	0.99995	0.04741	0.04708	-0.00033	0.70
4	Be III	0.99991	0.03538	0.03531	-0.00007	0.20
5	B IV	0.99985	0.02821	0.02824	0.00003	0.11
6	C V	0.99978	0.02346	0.02354	0.00008	0.34
7	N VI	0.99970	0.02008	0.02017	0.00009	0.45
8	O VII	0.99961	0.01756	0.01765	0.00009	0.51
9	F VIII	0.99951	0.01560	0.01569	0.00009	0.58
10	Ne IX	0.99939	0.01404	0.01412	0.00008	0.57
11	Na X	0.99926	0.01277	0.01284	0.00007	0.55
12	Mg XI	0.99911	0.01171	0.01177	0.00006	0.51
13	Al XII	0.99895	0.01081	0.01086	0.00005	0.46
14	Si XIII	0.99878	0.01005	0.01009	0.00004	0.40
15	P XIV	0.998596	0.009388	0.009415	0.000027	0.29
16	S XV	0.998397	0.008811	0.008827	0.000016	0.18
17	Cl XVI	0.998185	0.008303	0.008307	0.000004	0.05
18	Ar XVII	0.997960	0.007852	0.007846	-0.000006	0.08
19	K XVIII	0.997720	0.007449	0.007433	-0.000016	0.21
20	Ca XIX	0.997467	0.007088	0.007061	-0.000027	0.38

Table 3.  $-T_2$ 's calculated from the RRF with Equation (12) and with Equations (3) and (13) for the  $1s^2$  state of the He isoelectronic sequence with  $Z=1$  to 20 are listed together with experimental  $-T_E$ 's. Electron affinity of H is from Hotop and Lineberger<sup>9</sup>. All other energies are from Moore<sup>8</sup>. All energies are in  $\text{cm}^{-1}$ .  $\Delta T = -T_2 + T_E$ .  $\Delta T\% = 100|\Delta T/T_E|$ . (1 eV = 8065.479  $\text{cm}^{-1}$ ).

Z	$-T_E$	Equation (12)			Eqs. (3) & (13)		
		$-T_2$	$\Delta T$	$\Delta T\%$	$-T_2$	$\Delta T$	$\Delta T\%$
1	115761.85	115750	10	0.010	115760	0	0
2	637219.61	638380	1160	0.182	636910	-310	0.048
3	1597739.1	1598740	1000	0.062	1598440	700	0.044
4	2997278.1	2997680	400	0.013	2998330	1050	0.035
5	4836106.5	4835850	-260	0.005	4837230	1130	0.023
6	7114456	7113420	-1040	0.015	7115410	950	0.013
7	9832847	9831180	-1660	0.017	9833520	670	0.007
8	12991528	12989220	-2310	0.018	12001810	280	0.002
9	16591050	16588200	-2850	0.017	16590820	-230	0.001
10	20631881	20628690	-3190	0.015	20631250	-630	0.003
11	25114737	25111150	-3590	0.014	25113740	-1000	0.004
12	30040212	30036560	-3650	0.012	30038920	-1290	0.004
13	35409160	35405960	-3200	0.009	35407700	-1460	0.004
14	41222323	41219020	-3300	0.008	41220800	-1520	0.004
15	47480708	47478190	-2510	0.005	47479280	-1420	0.003
16	54185198	54183470	-1730	0.003	54184030	-1170	0.002
17	61336962	61336430	-530	0.001	61336220	-740	0.001
18	68937109	68937900	790	0.001	68937130	20	0
19	76986683	76989210	2530	0.003	76987680	990	0.001
20	85487155	85491820	4670	0.005	85489420	2270	0.003

average deviation : 0.021 0.010

Table 4.  $\mu^*$ 's are converted from experimental  $-T_E$ 's in Table 3 by using  $\sigma=0.225$ .  $\mu$ 's are calculated from Equations (3) and (13) with  $\mu=\beta(Z-\sigma)$  for  $Z=1$  and  $\beta^{1.02}/Z^{0.97}$  for  $Z>1$ .  $\Delta\mu=\mu-\mu^*$ .  $\Delta\mu\% = 100|\Delta\mu/\mu^*|$ .

Z	SPECIES	$\mu^*$	$\mu$	$\Delta\mu$	$\Delta\mu\%$
1	H <sup>-</sup>	0.06683	0.06683	0	0
2	He I	0.04166	0.04191	0.00025	0.60
3	Li II	0.02850	0.02828	-0.00022	0.77
4	Be III	0.02158	0.02140	-0.00018	0.83
5	B IV	0.01735	0.01723	-0.00012	0.69
6	C V	0.01451	0.01444	-0.00007	0.48
7	N VI	0.01247	0.01243	-0.00004	0.32
8	O VII	0.01093	0.01092	-0.00001	0.09
9	F VIII	0.009740	0.009744	0.000004	0.04
10	Ne IX	0.008782	0.008797	0.000015	0.17
11	Na X	0.008000	0.008020	0.000020	0.25
12	Mg XI	0.007350	0.007371	0.000021	0.28
13	Al XII	0.006800	0.006820	0.000020	0.29
14	Si XIII	0.006328	0.006347	0.000019	0.30
15	P XIV	0.005920	0.005936	0.000016	0.27
16	S XV	0.005565	0.005576	0.000011	0.20
17	Cl XVI	0.005252	0.005258	0.000006	0.11
18	Ar XVII	0.004973	0.004974	0.000001	0.02
19	K XVIII	0.004726	0.004720	-0.000006	0.13
20	Ca XIX	0.004505	0.004491	-0.000014	0.31

Table 5. Data for the  $C;[1s^2 2s^2] 2p^2$  isoelectronic sequence are shown. EQN's are from one-electron binding energies in Moore<sup>4</sup>. Experimental two-electron binding energies  $-T_E$  are from Moore<sup>5</sup> while the electron affinity of B is from Hotop and Lineberger<sup>7</sup>.  $\mu^*$ 's are converted from  $-T_E$ 's through Equation (1).  $\mu$ 's are calculated from Equations (3) and (15).  $-T_2$ 's are computed from the RRF in Equation (1) with  $\sigma=0.170$  and the calculated  $\mu$ 's. The split energy levels are designated in Equation (14).  $\Delta T$  and  $\Delta T\%$  are defined in Table 3. The (\*) associated with  $\Delta T$  indicates that the deviation is within experimental uncertainties. All energies are in  $\text{cm}^{-1}$ . ( $1 \text{ eV} = 8065.479 \text{ cm}^{-1}$ ).

Z	SPECIES	EQN	$\mu^*$	$\mu$	$-T_E$	$-T_2$	$\Delta T$	$\Delta T\%$
1	B <sup>-</sup>	1.28045	0.19754	0.19754	69190	69210	0*	0
2	C I	1.49394	0.10497	0.10564	287485.1	287245	240	0.084
3	N II	1.60642	0.07535	0.07576	621454	621150	300	0.048
4	O III	1.67689	0.05974	0.05984	1067470	1067340	130	0.012
5	F IV	1.72548	0.04996	0.04933	1624260	1624490	230	0.014
6	Ne V	1.76105	0.04307	0.04291	2291800	2292220	420	0.018
7	Na VI	1.78822	0.03794	0.03781	3070000	3070490	490	0.016
8	Mg VII	1.80958	0.03347	0.03346	3990000	3959410	300	0.008
9	Al VIII	1.82682	0.03081	0.03078	4980000	4958480	210	0.004
10	Si IX	1.84097	0.02827	0.02823	6069700	6069760	60*	0.001
11	P X	1.85275	0.02619	0.02617	7292000	7291640	360*	0.0005
12	S XI	1.86270	0.02431	0.02431	8627000	8625170	1830*	0.0002
13	Cl XII	1.87118	0.02269	0.02269	10074000	10071600	2400*	0.0002
14	Ar XIII	1.87844	0.02140	0.02140	11679000	11679900	900*	0.0008

Figure 1. Energy levels of  $[\text{core}]n_1l^2$  systems. For  $Z=1$  cases, this diagram depicts a positive electron affinity.

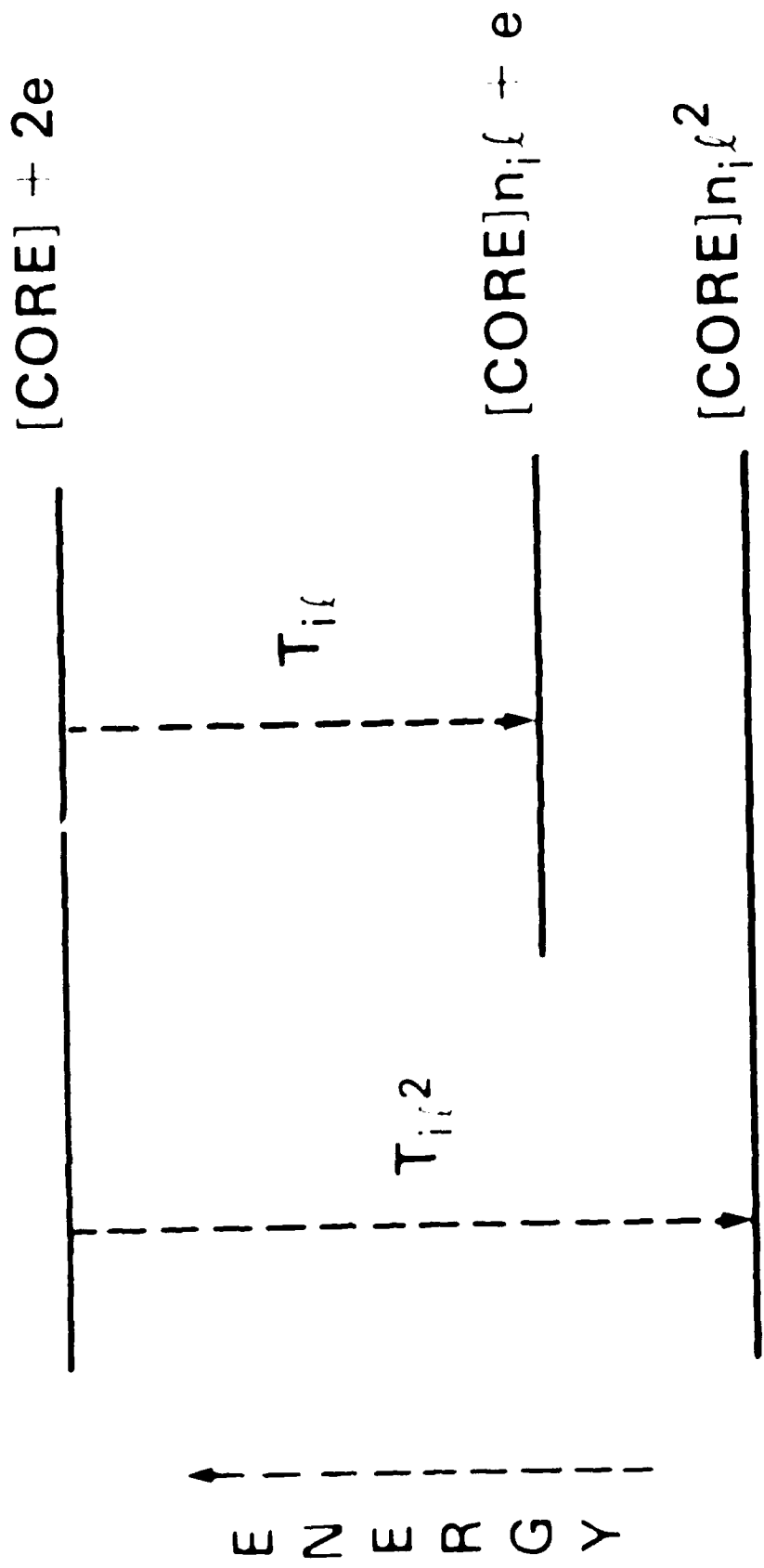


Figure 1

END

7-87

Dttic